



### Politecnico di Torino

Corso di Laurea Magistrale in Ingegneria Aerospaziale
A.a. 2025/2026
Sessione di Laurea ottobre 2025

# Comparison Between Parallel and Competitive Reaction Schemes for the Pyrolysis of Cork/Phenolic Ablators

Relatori:

Candidato:

Professore Domenic D'Ambrosio Professore Thierry Magin Francesco Spina

# Acknowledgements

It is difficult to express how grateful I am for the opportunity to conclude my academic journey with such a remarkable experience. Being part of the von Karman Institute for Fluid Dynamics has been an incredible experience, full of opportunities to learn, explore and engage my curiosity. Everyone, even those not directly involved in my work, has always been kind, open and ready to help.

I am thankful to Politecnico di Torino for the solid preparation it has given me over the past years, which allowed me to meet the standards required for this work.

I would like to thank Professor Thierry Magin for directing me toward this fascinating project during my application, and for suggesting new and stimulating topics when defining my thesis outline.

My gratitude also goes to Professor Domenic D'Ambrosio for his well-taught and engaging lectures which provided the foundations that made this experience possible.

A special thank you goes to Bernd, whose supportive and encouraging supervision contributed to the success of this thesis. His interest, constructive feedback and availability were particularly appreciated.

I am especially indebted to Diana for her guidance and support. She trusted my work, always found time to discuss my questions, and shared her knowledge with generosity to the small details that make the difference. She was key to the development of this thesis and to my personal growth.

Thanks to Simone for introducing me to TGA and for allowing me to take an active role in the experimental campaign. It is thanks to his explanations, time dedication and trust that the experimental part of this work was made possible and enjoyable.

Finally, I wish to express my gratitude to Professor Francisco Torres-Herrador, whose previous work laid a rigorous and inspiring foundation for mine. On the occasion we had to meet, his insight and help were remarkable. His research set a high standard that motivated me to improve my own. I was lucky to be able to work starting from such a solid and trustworthy foundation.

# **Abstract**

New challenges are emerging in the development of Thermal Protection Systems (TPS). The growing number of spacecraft in orbit, the renewed interest in human spaceflight, and advances in reusable components have increased the research focus on accurate material characterisation for a dual function. TPS materials must ensure protection during atmospheric entry and complete demise during disposal. In both cases, reliable prediction of thermal degradation is essential to optimise design margins and ensure system safety.

Cork is a promising material for TPS applications. Its cellular structure provides high porosity, low density, and excellent thermal insulation. These properties make cork a promising candidate to replace widely used carbon/phenolic composites. However, TPS materials degrade through pyrolysis, a complex thermochemical process whose modelling is only partially understood. The challenge of developing a robust thermal degradation model for this phenomenon is increased by the limited literature available on cork. This is in contrast to the extensive studies conducted over the past decades on other types of biomass and carbon/phenolic composites.

Previous studies have investigated pyrolysis modelling of carbon/phenolic composites at the von Karman Institute. In particular, the work of Torres-Herrador served as a primary reference for this work. Building on the developed methodology for extracting kinetic parameters, this thesis applies a similar approach to cork/phenolic composites, focusing on model fitting methods rather than isoconversional techniques. This work aims to propose a pyrolysis scheme for cork/phenolic materials by comparing parallel and independent reaction formulations, commonly used in the ablation community, with competitive reaction mechanisms.

This work was divided into two phases. First, an experimental campaign based on Thermogravimetric Analysis (TGA) was conducted on two different cork/phenolic ablators at three heating rates (5, 20, and 40 K/min). Second, parallel and competitive reaction models, based on Arrhenius-like kinetics, were proposed to describe the thermal degradation of each material. Kinetic parameters were identified using deterministic optimisation to achieve the best fit with experimental data. The optimised parameters are intended as input for material response codes such as the Porous Material Analysis Toolbox (PATO) developed by NASA Ames. Accurate pyrolysis modelling is expected to significantly enhance the fidelity of such simulations and support the optimisation of TPS design.

The experimental results highlighted differences in degradation behaviour between

the two materials, despite the similarities in their constituents. Both materials presented a shift towards higher reaction temperatures as the heating rate was increased. It is known that parallel reaction schemes are not capable of adapting to heating rates relevant to TPS applications when optimised in the limited range of the presented data. This is caused by their inability to correctly represent the behaviour of several reactions occurring simultaneously and in competition for the same reactant, as seen in the shifting of reaction temperatures. Nonetheless, these models provided satisfactory agreement with TGA data in the analysed range. Developing a competitive reaction scheme for cork/phenolic composites proved to be more difficult due to the complexity of the material and the lack of supporting literature. The results obtained are promising, but not yet sufficient to provide a fully reliable description of the underlying processes.

# Contents

Li	st of	Figures	VII
Li	st of	Tables	IX
N	omer	nclature	X
$\mathbf{A}$	crony	yms	XII
1	Intr 1.1 1.2 1.3	Protection and demise: the dual role of Thermal Protection Systems The importance of accurate modelling for atmospheric entry Objectives and outline of the thesis	1 1 4 5
2	Phy 2.1	Cork/phenolic ablators	7 9 10 10 12 13
3	<b>Kin</b> 3.1 3.2	Multi-component mechanisms	1 <b>7</b> 17 19
4	Mat 4.1 4.2 4.3	terials and methods  Materials  Experimental methodology  4.2.1 Sample production  4.2.2 Post-processing of the experimental data  Arrhenius parameters optimisation: Pyropy  4.3.1 Model calibration: Shuffled Complex Evolution algorithm	20 21 24 27 29 32
5	Res 5.1 5.2	sults and discussion  Experimental TGA results	34 34 47

	5.3	Competitive reactions model	50
6	Cor	nclusions and future developments	55
	6.1	Recommendations for future developments	57

# List of Figures

$1.1 \\ 1.2$	QARMAN mission	$\frac{2}{2}$
1.3	Plasmatron test	3
2.1	Schematic of pyrolysis zones	8
2.2	Section of a sample post Plasmatron testing	9
2.3	Thermal evolution of phenolic resin	11
2.4	TGA/DTGA results exemplification	14
2.5	STA apparatus and main components	15
2.6	Photos: VKI STA facility	16
3.1	Solid sub-phases in parallel mechanisms	17
4.1	Temperature profile of dynamic TGA	21
4.2	Photo: Cork 2 powdering process	24
4.3	Photo: mould	25
4.4	Photo: virgin and charred samples	26
4.5	Photo: sample-crucible setup	27
4.6	Pyropy optimisation flowchart	33
5.1	Experimental TGA data of Cork 1	35
5.2	Experimental TGA data of Cork 2	36
5.3	Experimental DTGA data of Cork 1	38
5.4	Experimental DTGA data of Cork 2	39
5.5	Additional TGA/DTGA of Cork 2	40
5.6	Reidual mass comparison	41
5.7	Shifting of TGA/DTGA	42
5.8	TGA for moisture removal	43
5.9	TGA/DTGA for moisture removal	44
5.10	Open/close glovebox comparison	45
	Paralle model results for Cork 1	48
	Paralle model results for Cork 2	49
	Competitive model for biomass	50
5.14	Competitve model for phenolic resin	50

5.15	Developed biomass/phenolic competitive model	51
5.16	Biomass/phenolic model results for Cork 1	52
5.17	TH competive model results for Cork 1	53

# List of Tables

4.1	Codes of experimental runs	23
4.2	Average of samples masses	26
5.1	Kinetic parameters for Cork 1 (multi-component model)	47
5.2	Kinetic parameters for Cork 2 (multi-component model)	48
5.3	Kinetic parameters for Cork 1 (biomass/phenolic model)	52
5.4	Kinetic parameters for Cork 1 (TH model)	53

# Nomenclature

### Greek Symbols

$\alpha$	Advancement of reaction	[-]
β	Heating rate (for optimisation: K/s)	[K/min]
$\gamma$	Mass coefficients	[-]
ρ	Density	$[{ m kg/m^3}]$
$\sigma$	Standard deviation	[-]
au	Weighting factor	[-]
ζ	Stoichiometric coefficient	[-]

### Roman Symbols

$\mathcal{A}$	Pre-exponential factor	[1/s]
A	Optimisation parameter	[-]
A	System (kinetic) matrix	
${\cal E}$	Activation energy	$[\mathrm{kJ/mol}]$
F	Mass-loss fraction	[-]
$I_n$	Identity matrix	
J	Jacobian matrix	
k	Reaction rate	
m	Normalised mass fraction	[%]
n	Order of reaction	[-]
p	Parameter for optimisation	
p	Parameter vector	
R	Gas constant	$[\mathrm{J/mol/K}]$
$S(\mathbf{p})$	Objective (misfit) function	[-]
t	Time	[s]
T	Temperature	[K]
W	Weighting matrix in the least-squares norm	[-]

### Indices

- 0 Initial conditions
- $\infty$  Final conditions
- ad Admissible
- best Best set
- cons Consumption
- G Gas phase
- prod Production
- obs Observations
- r Reaction
- rep Repetitions

# Acronyms

**DSC** Differential Scanning Calorimetry

**DTGA** Differential Thermogravimetric Analysis

EA Elemental Analysis

ESA European Space Agency

FiTGA Fitting TGA Algorithm (legacy Matlab tool)

FTIR Fourier Transform Infrared Spectroscopy

GA Genetic Algorithm

**Gpyro** General Pyrolysis Solver (University of Arizona)

IVP Initial Value Problem

IXV Intermediate eXperimental Vehicle

MLR Mass Loss Rate

NASA National Aeronautics and Space Administration

PATO Porous media Analysis Toolbox based on OpenFOAM

PICA<sup>®</sup> Phenolic Impregnated Carbon Ablator

QARMAN QubeSat for Aerothermodynamic Research and Measurements on AblatioN

RMSE Root Mean Square Error

SCE Shuffled Complex Evolution

SG Savitzky–Golay

SLA Super Light Ablators

STA Simultaneous Thermal Analysis

 ${\bf TGA} \qquad \qquad {\bf Thermogravimetric\ Analysis}$ 

TPS Thermal Protection System

VKI von Karman Institute for Fluid Dynamics



# Chapter 1

# Introduction

# 1.1 Protection and demise: the dual role of Thermal Protection Systems

Atmospheric entry produces hypersonic flows with strong shock heating and radiative/convective loads that would exceed structural temperature limits of spacecrafts lacking a dedicated thermal barrier. A Thermal Protection System (TPS) is the engineered protective layer that ensures survival along the mission design planned trajectory by redistributing, absorbing, and removing heat before it reaches the sub-structure. In ablative systems, heat rejection is achieved through endothermic pyrolysis, in-depth gas transport, and surface or volume mass removal (char oxidation, sublimation, spallation). Beyond protection, modern space-safety requirements make TPS behaviour during disposal equally relevant: materials must degrade in a controlled and predictable manner to guarantee on-orbit demise and compliant ground risk.

Within available ablative materials, carbon/phenolic systems have been more commonly adopted due to their relatively simple phenomenology — characterised by the absence of bulk swelling, the presence of a stiff preform, and the availability of extensive legacy datasets — which greatly facilitates both modelling and validation [1, 2]. An alternative is represented by cork/phenolic systems, which combine very low weight and conductivity with a cellular microstructure that is compressible and gas-permeable.

Despite these challenges, cork/phenolic materials are already used in flight hardware and demonstrators. The material that will be referred to as Cork 1 in this thesis, for example, was used for the activities of the QARMAN re-entry CubeSat (Figure 1.1) developed at the von Karman Institute for Fluid Dynamics (VKI) [3–6]. For this mission (flown in the early 2020s), Cork 1 constituted the front heatshield, which hosted thermocouple plugs at multiple depths and pressure ports to characterise heating, in-depth response, and recession [7].





Figure 1.1: QARMAN mission outline and TPS test in Plasmatron.

Credit: ESA and VKI.

Cork 1 was also integrated as part of the Intermediate Experimental Vehicle (IXV) project (Figure 1.2a). ESA developed a lifting-body re-entry demonstrator conceived to validate aerothermodynamics, TPS, and guidance—navigation—control in a representative hypersonic environment [8]. In the past, other missions and launch systems, of both ESA and NASA, benefited from a Cork 1-based TPS [9]. Some of these are shown in Figure 1.2.



(a) ESA's IXV project



(b) Cork-based thermal protection for rocket nozzles.

Figure 1.2: Examples of past mission utilising Cork 1 based TPS.

Credit: Amorim Cork Solutions.

In more recent times, space-safety initiatives pursue design-for-demise (D4D) development. Indeed, due to the interest in contrasting the increasing quantity of space debris, missions like ESA's DRACO (Destructive Reentry Assessment Container Object) were conceived. The mission design involves a host satellite guided to destructive re-entry while an internal capsule, equipped with thermal and structural sensors, attempts to transmit in-flight breakup data. The internal capsule acts similarly to an

aeroplane's black-box and needs to survive re-entry. During the design phase at VKI, Cork 1 has been selected as the material for the TPS of Draco's internal capsule [10].

Over time, VKI has accumulated specific know-how on cork/phenolic ablators through QARMAN and, more recently, DRACO. This expertise is supported by repeated campaigns in the Plasmatron inductively coupled plasma wind tunnel, shown in Figure 1.3 [3, 5]. This facility provides well-controlled, high-enthalpy experimental conditions for material-response observation and model calibration. Additionally, several campaigns at VKI's Simultaneous Thermal Analyser (STA) facility built extended experience on kinetic characterisation of pyrolysing materials [1, 11].

The present work benefits from this knowledge and focuses on the kinetic modelling aspects required to make the most effective use of cork/phenolic advantages in both protection and demise scenarios.

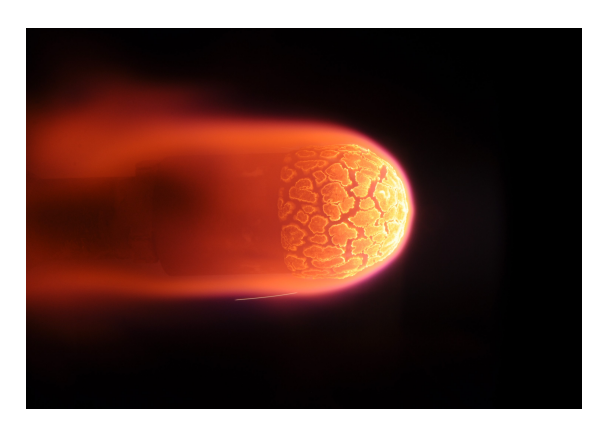


Figure 1.3: Cork/phenolic ablator tested in Plasmatron. Courtesy of VKI  ${\it Credit:} \ {\it VKI}.$ 

# 1.2 The importance of accurate modelling for atmospheric entry

Cork/phenolic ablators are challenging to model because several tightly coupled processes occur over overlapping temperature ranges. Thermo-chemically, multiple constituents react simultaneously (suberin, lignin, cork polysaccharides and phenolic resin), with consecutive and competitive pathways that depend on temperature and heating rate. Products undergo devolatilisation, cross-linking, and char formation while permeability and porosity change over time. When cork begins to pyrolyse, the solid matrix decomposes into solid char and gaseous volatiles. These gases are generated inside the porous network faster than they can escape. Since cork has a closed or semi-closed cell structure, this leads to a pressure build-up inside the cells and microvoids, causing expansion (swelling) of the bulk material. As pyrolysis continues, the cell walls degrade, the solid mass fraction decreases, leading to the collapse of the microstructure, and gases eventually escape through new cracks or pores. Once gases escape, internal pressure drops, and the remaining char contracts (shrinkage). Numerically, these couplings create moving boundaries, evolving properties, and non-unique kinetic parameter sets if identification is not carefully constrained across rates and regimes [5, 6, 12, 13].

A robust model for the numerical simulation of cork/phenolics ablative materials would have numerous significant benefits:

- Robust models across regimes. Consistent kinetics valid over wide heating-rate ranges reduce extrapolation error during the design phase.
- Lower design margins. Reduced model uncertainty justifies smaller thermal and structural safety factors, directly decreasing mass.
- Fewer experimental tests. Numerical simulation would replace a significant portion of plasma-tunnel tests, focusing experimental budget on validation.
- Exploit cork. By correctly capturing swelling, gas percolation, and shrinking, designs can leverage the benefits of cork/phenolic ablators.

With today's limited simulation capability for cork/phenolics (especially the concurrent swelling—shrinking behaviour and overlapping competitive kinetics), mission design often depends on extensive, expensive experimental campaigns to test design options. Additionally, experimental results confidence remains bound by the limited tested envelope compared to real in-flight conditions. For this reason, high safety factors are imposed to mitigate uncertainty. All of this results in increased cost and excess mass.

For all these reasons, this work goal is to contribute to an improved thermo-chemical model with research on the kinetic decomposition of phenolic resin, biomass and cork. Considering the scarce literature on cork/phenolic materials, a new reaction mechanism for pyrolysis would provide an important foundation for future improvements of their numerical simulation.

### 1.3 Objectives and outline of the thesis

This thesis addresses the modelling choices that currently limit the predictive fidelity of cork/phenolic ablators by combining multi-rate TGA data with deterministic parameter identification. The intended aim is to obtain kinetic parameters and solid yields that can be used in porous-material solvers for TPS studies at high heating rate conditions. As an end-use example, experimentally validated parameter sets are conceived as improved inputs for the Porous Material Analysis Toolbox based on OpenFOAM (PATO) used at VKI, thereby enhancing numerical design studies. Taken together, these considerations motivated the following question.

Is it possible to develop a reaction mechanism, calibrated on multi-rate TGA/DTGA, capable of modelling degradation of cork/phenolic TPSs, both at laboratory and flight-representative heating rates?

From this initial input, during the research work, more detailed objectives were set:

Objective 1. Establish a reliable calibration basis at laboratory heating rates. Build a multi-rate TGA/DTGA dataset (5, 20, 40 K/min) for two cork/phenolic ablators (Cork 1 and Cork 2).

Objective 2. Determine a kinetic mechanism that supports the temperature- and time-dependent behaviour of  $\operatorname{cork/phenolic}$  materials, improving and refining the  $\operatorname{Py-ropy}$  package for the task. Within a unified optimisation and scoring framework, compare multi-component (parallel) and competitive mechanisms. Using the experimental dataset and the correct reaction mechanism, identify Arrhenius parameters and solid-yield fractions that are stable across rates.

Objective 3. Analyse material-specific behaviour under common experimental conditions. Using the same TGA/DTGA experimental procedure, post-processing workflow and optimisation, compare Cork 1 and Cork 2 to quantify differences in onset temperatures, peak mass-loss rates and residual char.

### Outline of the thesis.

The thesis starts by reviewing the physics of porous ablators with emphasis on cork/phenolic systems and the role of heating rate in thermal decomposition in Chapter 2. A dedicated chapter (4) presents the Thermogravimetric Analysis methodology used to generate the calibration and validation dataset. The kinetic-modelling section, Chapter 3, formalises the multi-component and competitive frameworks and their governing equations. The materials and methods are described next, including the multi-rate experimental campaign, data-reduction procedures, the optimisation workflow for parameter identification, and the Shuffled Complex Evolution algorithm, Chapter 4. The results and discussion, Chapter 5, reports experimental trends, fitted models, and a cross-comparison of mechanisms and materials, with attention to cross-rate consistency. The thesis concludes by summarising how Objectives were addressed and by providing recommendations for future work.

# Chapter 2

# Physics of porous ablative materials

Pyrolysis is the endothermic thermo-chemical process by which the organic matrix of a charring ablator decomposes into a carbonaceous residue (char) and volatile products. A relevant key feature is the flow of pyrolysis gases through the pore network of the charred layer, which absorbs thermal energy and can trigger secondary reactions. In lightweight porous systems, heat and mass transfer are tightly coupled: density, conductivity, permeability and porosity evolve continuously as virgin material is converted into char, while the generated gases convect through the pores and may react or coke within the hot porous solid structure of the char zone. In most material-response formulations, the pyrolysis gas is treated (at the macroscale) as a single, non-reactive species in thermal equilibrium with the solid; gas flow in the pores is commonly modelled with Darcy's law, and properties across the virgin—char transition are interpolated using an extent-of-reaction variable. These modelling hypotheses are introduced and motivated in the lectures and notes of the Hypersonic Aerothermodynamics course at Politecnico di Torino [14].

A convenient description for flight conditions of a TPS is by a multizone structure (see Fig. 2.1) where all zones coexist while the thermal front moves inward. Three layers overlaid in a direction normal to the free-flow/TPS interface can be identified [14, 15]. The TPS is usually bound to a sub-structure that represents the system benefitting from the thermal protection.

Ablation zone (receding surface). The outermost char, directly exposed to the boundary layer, reaches the highest temperatures. Material is removed by oxidation, sublimation, and spallation; radiative exchange is intense, and the strong outflow of pyrolysis gases provides boundary-layer blowing that reduces convective heat transfer.

Char zone. Beneath the surface, the carbonised skeleton is highly porous and exhibits altered thermophysical properties (typically higher permeability/porosity and modified

conductivity/emissivity). Pyrolysis gases produced in the pyrolysing zone, pour through this layer, where they may coke or participate in secondary gas—solid reactions.

**Decomposition (pyrolysis) zone.** In this zone, the material encounters the temperature window in which the polymeric binder (and biomasses) depolymerises and carbonises. The local density drops while shrinkage (and possibly swelling of cork) occurs; volatile products are generated and driven outward by pressure gradients, contributing to in-depth convection.

**Virgin composite.** The intact cork/phenolic retains its unaltered properties. Heat is transported primarily by conduction until the local temperature rises enough to trigger decomposition, advancing the pyrolysing front.

**Sub-structure.** The load-bearing substrate lies beneath the TPS and does not participate in pyrolysis. Its thermal state is a primary design constraint: the central objective of the TPS is to keep the sub-structure below its allowable temperatures throughout atmospheric entry.

This zonal view clarifies how pyrolysis simultaneously absorbs energy (bond scission, gas heating) and removes energy (ablation and boundary-layer blowing) to protect its sub-structure from elevated temperatures [14].

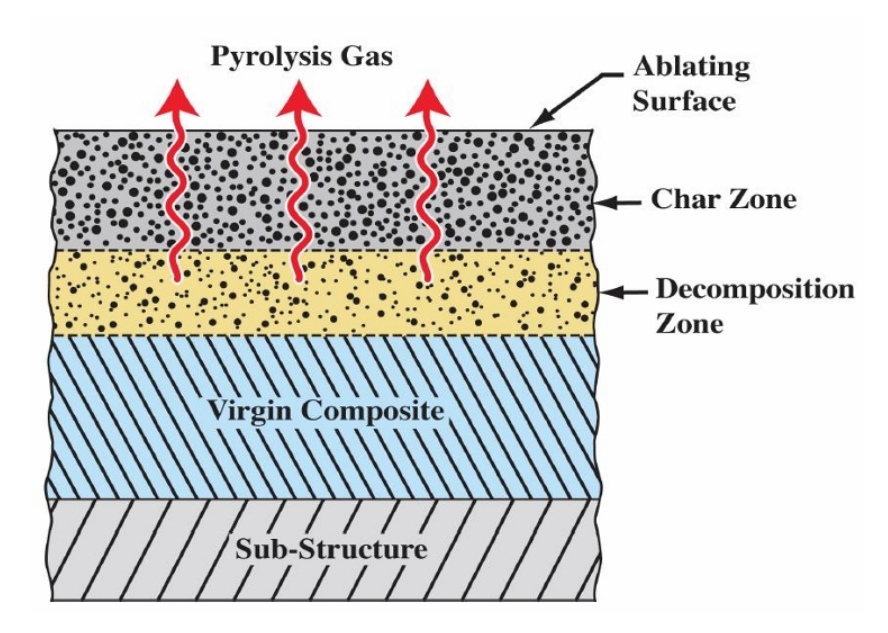


Figure 2.1: Schematic of the multizone structure of an ablative TPS undergoing pyrolysis. Highest to lowest temperature: ablation surface, char zone, pyrolysis layer, virgin composite, and sub-structure. Courtesy of [15].

### 2.1 Cork/phenolic ablators

During pyrolysis, phenolic-based ablative materials experience a notable volumetric contraction. This shrinkage results from the breakdown of organic constituents and the release of volatile compounds, which lead to a progressive densification of the remaining carbonaceous matrix. In cork/phenolic systems, however, a transient swelling (or foaming) can precede or overlap the onset of net contraction. The extent of shrinkage and swelling depends on the initial porosity and cork/resin content, and it is often accompanied by surface cracking and visible mass loss. These effects add great complexity to the understanding of the morphological evolution and performance of porous thermal protection materials under high-temperature conditions [12, 13]. The pyrolysis gases' pressurisation that drives swelling causes a boundary-layer displacement that distances the heat front from the sub-structure. These types of advantages make cork/phenolic attractive, but they also complicate prediction in numerical frameworks originally tuned to non-swelling materials. Net shrinkage and the multizones pattern depicted in Section 2 can be clearly identified in charred cork/phenolic samples after testing in the VKI Plasmatron (high-enthalpy plasma wind tunnel) and by comparison with virgin samples, Figure 2.2.

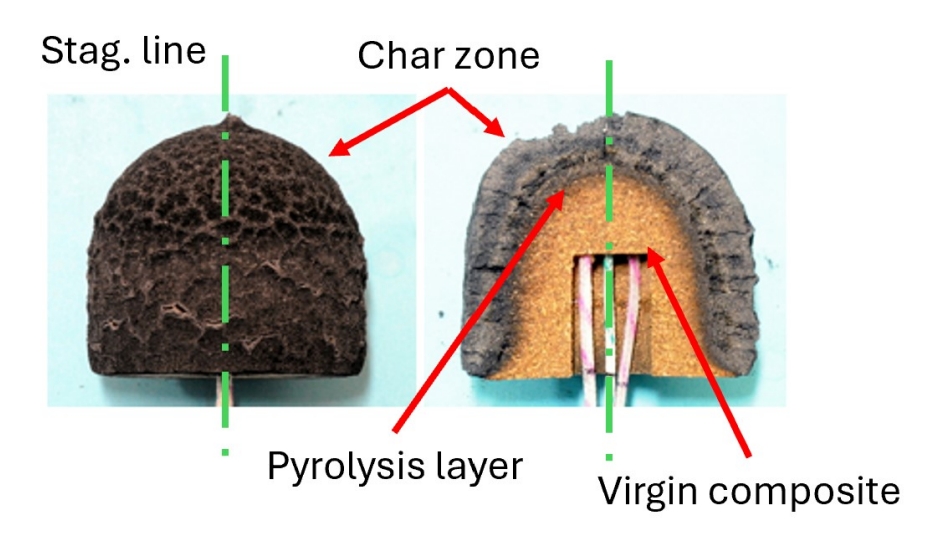


Figure 2.2: Pyrolysis zones in a partially charred cork/phenolic sample after testing in plasma flow. Adapted from [3].

Charring ablators are typically heterogeneous composites consisting of (i) a low-density, porous reinforcement or filler phase (e.g. carbon fibres or natural cork granulate) and (ii) a thermoset binder. This diversity of constituents implies multiple, overlapping thermo-chemical pathways during heating [1, 14]. But cork/phenolic materials are intrinsically more complex than carbon/phenolic ablators: whereas carbon/phenolic includes an essentially non-pyrolysing, inert component (carbon fibres) [16], cork/phenolic presents simultaneous pyrolysis decomposition of cork and resin. Cork is itself a

composite, in which cellulose, hemicellulose, and lignin (fibre-like constituents) are embedded in a suberin-rich matrix (matrix-like constituent) [17, 18]. All its components react in competition across partially overlapping temperature windows. This complexity motivates the separate discussions in Sections 2.1.1 and 2.1.2.

### 2.1.1 Pyrolysis of cork

While extensive literature exists on biomass pyrolysis for bioenergy and biogas production applications, cork represents a distinctive (rarely investigated) case within this broader category [18]. Indeed, its unique biochemical composition significantly differentiates it from conventional wood biomass [19]. Unlike typical lignocellulosic materials, where cellulose, hemicellulose, and lignin constitute the primary structural components, cork is characterised by a high content of suberin. Suberin is a hydrophobic polyester that serves as the predominant structural component. Different weight compositions (a characteristic that changes across cork species [20]) of cork have been measured with similar results [17, 21–23]: at over 40% of the total dry weight, suberin is the main element, followed by lignin (20-30%), polysaccharides including cellulose and hemicellulose (10-20%), and extractives (10-15%).

The thermal decomposition of cork proceeds through multiple overlapping stages that reflect the sequential degradation of its various biochemical constituents. Initial mass loss occurs between 50-200°C due to moisture evaporation and volatile release from extractives [21]. The primary decomposition phase initiates around 200°C with the degradation of hemicelluloses and extractives, followed by cellulose decomposition in the temperature range of 315-400°C with a peak temperature at approximately 355°C [20, 21]. Lignin degradation occurs across a broader temperature spectrum, beginning at ambient conditions and continuing up to 600°C, while suberin (the most thermally stable component) undergoes decomposition primarily between 390-525°C [17].

In two distinct studies, Şen [18] and Ghonjizade-Samani [17] analysed the contributions of cork's constituents to its thermal degradation. The removal of suberin from cork samples demonstrates its critical role in thermal stability: desuberized cork shows a major mass loss peak at 270°C—approximately 130°C lower than intact cork—confirming suberin's stabilising effect on the overall thermal behaviour [17]. Additionally, extractives exhibit a catalytic effect on cork's thermal decomposition, particularly between 200-300°C and again between 500-800°C, promoting slightly enhanced decomposition rates compared to extractive-free samples [17].

### 2.1.2 Pyrolysis of phenolic resins and derived composites

Composite materials relying on a phenolic-based matrix are widely employed in the aerospace field as key constituents of TPSs. Owing to this and many other applications, their thermal degradation behaviour has been extensively studied in the last few decades. Nonetheless, inconsistencies have been reported. As analysed in Section 2.1.3, the main reason for this difficult-to-predict thermal evolution is that these materials can attain distinct chemical states at the same temperature, making their degradation dependent

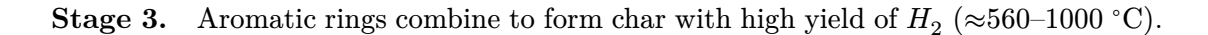
on both temperature and heating rate, as originally discussed by Stokes [24].

In general, Bessire and Minton [25] have identified a four-stage thermal evolution with overlapping temperature ranges (Fig. 2.3) for the pyrolysis of phenolic resins used in carbon/ and cork/phenolic ablators. The following Section synthesises phenolic resins thermal degradation process studied during mass-spectrometric campaigns on PICA® at vacuum/low-pressure conditions and flight-relevant heating rates by Bessire and Minton [26]. Indeed, PICA® (Phenolic Impregnated Carbon Ablator) is a carbo/phenolic composite developed by NASA over 40 years ago [27].

**Stage 0.** Outgassing ( $\leq 400^{\circ}$ C). Trapped gases and moisture evaporate, only affecting the initial mass trace. A similar phase was recorded for Cork 2, Section 5.1.

Stage 1. As the temperature rises it is now sufficient for depolymerisation of the phenolic resin to start ( $\approx 200$ –550 °C). Phenol and derivatives are produced, with major volatilisation of  $H_2O$ .

Stage 2. Cross-links breakdown produces  $H_2$ , CO and  $CH_4$  as main products ( $\approx 400-800$  °C). As the heating rate increases, CO generally decreases and  $CH_4$  increases [26].



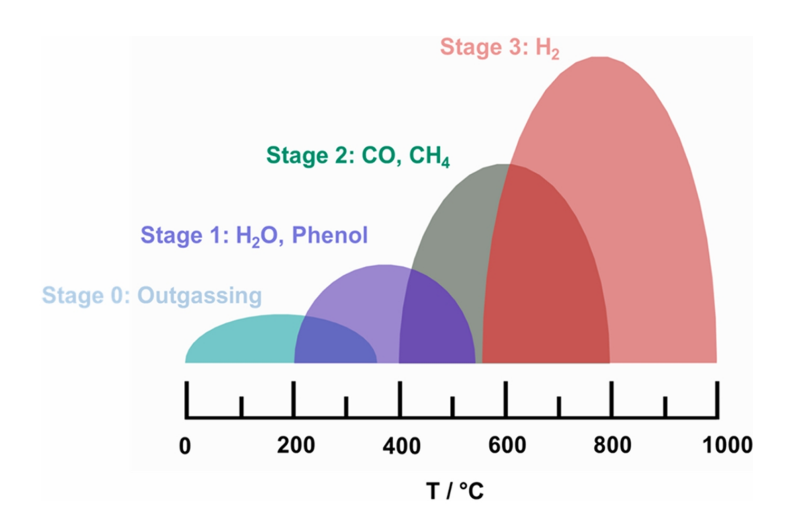


Figure 2.3: Four-stage thermal evolution of phenolic resin: Stage 0 (Outgassing), Stage 1 (Depolymerisation), Stage 2 (Cross-links breakdown) and Stage 3 (Char formation), mapped qualitatively versus temperature. Courtesy of [25, 26].

In a composite ablator, these resin-driven reactions unfold within the porous structure. The resulting pyrolysis gases flow outward through the growing char layer, where secondary reactions and boundary-layer chemistry may further transform species [25, 26].

Cork's multi-component competitive degradation behaviour necessitates sophisticated modelling approaches that account for the competitive and consecutive reactions occurring across overlapping temperature windows. A complexity that extends beyond conventional single-component biomass pyrolysis models and is enhanced by the simultaneous degradation process of phenolic resin. The combination of these two constituents' thermal behaviour directly influences the performance of cork/phenolic ablators under high-temperature aerospace applications.

### 2.1.3 Time and temperature dependent behaviour

The heating rate dependent behaviour of thermal decomposition is well documented both for cork and phenolic matrix based composites for aerospace applications [11, 19, 21]. It can be justified by the variation in the time available for molecular chains to accumulate sufficient energy to break their bonds [28]. This phenomenon results in a shift of the pyrolysis reactions towards higher temperatures, up to heating rates in the region of 100 K/min. At even higher heating rates, this trend is then reversed in both constituents of the ablator.

Indeed, at different heating rates, a change in the kinetics affects the degradation of components. Cork could be considered a composite material itself, in which many compounds (suberin, lignin, polysaccharides, etc.) react in the same range of temperatures. These various reactions are thought to compete, and temperature and time can change which one prevails. This switching to different kinetic pathways under diverse heating conditions has been proven for carbo/phenolic composites and is better described by models based on competitive reaction mechanisms [1].

Şen et al. [18] also addressed the combined effect of time and temperature on the thermal evolution of biomasses. The change from direct to inverted dependency between heating rate and temperature of reaction was explained with an initially preponderant "time effect" that gives way to a prevailing "temperature effect" over 100 K/min.

In the spectrum of high heating rates, similar to those experienced during atmospheric entry, the shifting of mass loss curves of carbon/phenolic ablators is partially attributed to measurement discrepancies due to the sample-crucible-thermocouple system [26]. These testing conditions are well outside of the operating range of the Netzsch STA analyser employed (NETZSCH STA 449 F3 Jupiter<sup>®</sup>). Additionally, temperature gradients are strongly dependent on the type of material and reaction rates [29]. For these reasons, it is difficult to evaluate the impact of temperature lags between the sample and the crucible on this work.

Heating rate does not appear to consistently affect the final char yield for either cork or phenolic resins. Minor fluctuations in cork residual mass (increasing with the heating rate) have been reported in literature, and attributed to a different activation behaviour of polysaccharides with increasing heating rate [18].

For cured phenolic resins, Stokes [24] observed a limited decrease of residual mass at increasing heating rates (up to and over 1000 K/min). His study is not the only one indicating this decrease at high heating rates, but opposite evidences in the literature were highlighted in the same article.

Both cork's and phenolic resins' char yields exhibit uncertain and sometimes contradictory responses to heating rate when studied separately. Unfortunately, no published studies were found addressing this effect in cork/phenolic ablators. In a composite, interactions between the two phases could further modify these trends during simultaneous degradation.

The weight ratio between cork and resin is therefore a critical parameter: if both constituents follow similar tendencies, their effects may add up, whereas opposite behaviours could partially cancel out. The overall response should be expected to be influenced mainly by the component with the higher weight fraction in the virgin composite. This cannot be stated with certainty, but it is an assumption supported by the fact that neither material alone has shown a sufficiently strong or consistent trend to guarantee dominance even when present in lower proportions.

### 2.2 Technique: Thermogravimetric Analysis

A common technique to evaluate thermal properties of porous materials undergoing pyrolysis is Thermogravimetric Analysis (TGA). It is usually coupled with Differential Scanning Calorimetry (DSC) in a Simultaneous Thermal Analyser (STA) apparatus. In this thesis, the DSC capabilities of the facility were not exploited.

TGA monitors the mass evolution of a sample as a function of time and temperature when it is subjected to a programmed heating procedure. The one used in this work is depicted in Figure 4.1. For dynamic TGA, temperature is increased at a constant heating rate  $(\beta)$ , generally limited to 50 K/min.

When materials' kinetics depend on both temperature and time, more than one heating rate can be selected to enhance the significance of the experiment outcome. The selected heating rate is closely linked to the sample mass and significantly influences final results. The sample must experience a homogeneous temperature during the heating process; as a general guideline, the larger the sample, the slower the heating rate [2].

Heating the studied material will stimulate a sequence of physical and chemical transformations. Generally, the generation of volatile compounds through these reactions causes a measurable decrease in the sample mass. A balance and thermocouples monitor these parameters with high precision.

The recorded mass (or density) loss is typically plotted on temperature, producing a thermogram. Distinct slopes in the TGA curve can be interpreted as different steps of the thermal degradation process and are associated with pyrolysis reactions [22, 31]. To better identify major reactions, the derivative of the mass loss curve (DTGA) is computed. The resulting peaks indicate reaction events; however, in complex materials, multiple reactions may occur simultaneously.

To improve the clarity of the process described above, an explicatory graph is presented with dummy data in Figure 2.4 adapted from [30]. Distinct slopes of the TGA curve (blue) identify two different phases of the thermal degradation, contributing respectively to 25% and 50% of total mass loss. In red, the derivative of the mass loss (DTGA) exhibits two peaks. A peak's maximum usually corresponds to the highest

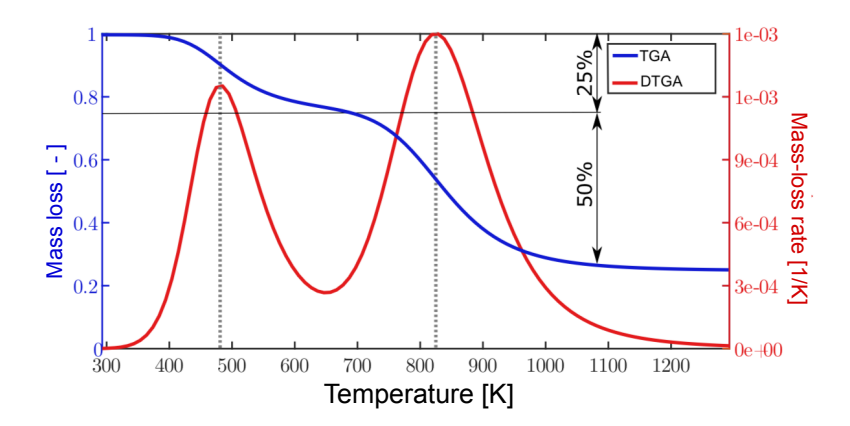


Figure 2.4: Dummy data representation of a typical TGA experiment. Two main reactions/decomposition stages can be identified by the DTGA (red) peaks. Adapted from [30]

intensity of a reaction.

When reactions overlap over the same temperature range, the inherent functioning of TGA prevents their separate identification. Indeed, TGA alone does not provide information on the underlying physical or chemical mechanisms. For this reason, it is often complemented by other experimental techniques. Examples can be found in the works of Torres-Herrador [1], Foster [22], Smith [32] and Ghonjizade-Samani [17]). For this same thesis project, the use of TGA as the sole source of experimental data imposed some limitations on the analysis capabilities.

Finally, when performing TGA experiments, it is essential to take into consideration the impact of the buoyancy effect (Archimedes' principle), which acts on the crucible and the sample and causes an apparent mass increase. To correct for this distorting action, a blank (baseline) run is recorded before every measurement (Section 4.2).

A detailed schematic of the main components of a TGA apparatus is illustrated in Figure 2.5. A brief description of the functions of the listed parts follows:

- Furnace / Temperature programmer: programmable heating chamber which operates following the experiment temperature profile.
- Sample holder: crucible where the samples are located.
- Reference crucible: empty crucible used to correct for buoyancy and baseline drift.

- Thermocouples: temperature sensors positioned on the crucible carrier. They measure the temperature difference between sample and reference.
- Purge gas: controlled and constant flow of inert or reactive gas that defines the atmosphere and carries evolved species out of the system.
- Balance: high-sensitivity microbalance with g resolution (Figure 2.6b).
- Radiation shields: reflective screens that reduce radiative heat transfer towards the balance.

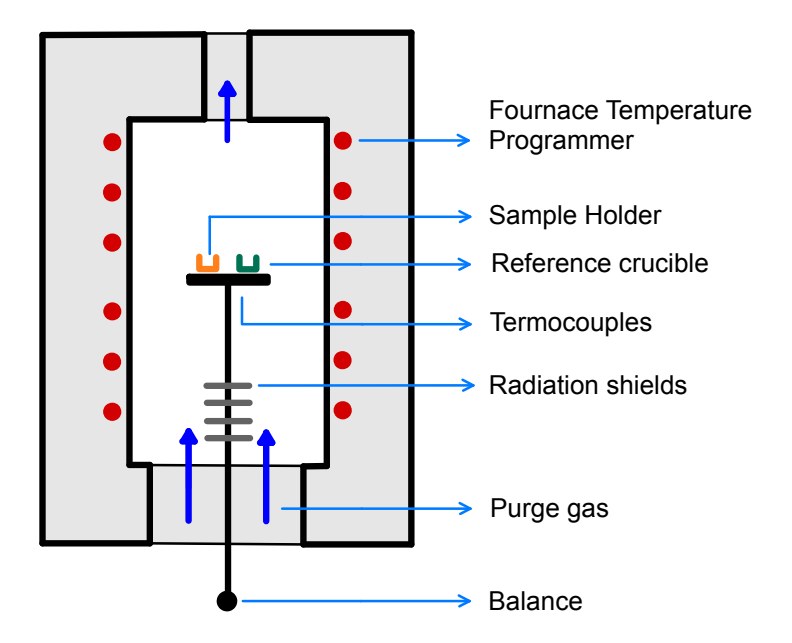


Figure 2.5: Schematic of STA apparatus and its main components.

Note that crucibles can be made of different materials. The shape and material of the one used in this campaign are detailed in Section 4.2. During TGA, the reference crucible was left empty for all the experimental runs. For this reason, even if always present, it will no longer be mentioned in the continuation of this work.

The purge gas is another parameter that is selected depending on the type of study. In this case, to analyse behaviour under pyrolysis, an inert gas (Argon) was used. On the contrary, for example, a study on combustion will require the presence of oxygen (or air) in the gas flow.

The thermal analyser used in this thesis is a NETZSCH 449 F3 Jupiter. The VKI laboratory features a glovebox in which the STA apparatus is located (Figure 2.6a). The glovebox creates a strictly controlled atmosphere in which the experiments are carried out, monitoring temperature, pressure and species composition (limited  $O_2$ ,  $H_2$  and  $H_2O$ ).

The controlled environment is also ideal for the storage of samples to avoid contamination and moisture absorption.

Unfortunately, during the majority of this project work, the glovebox was open. Having the STA apparatus in ambient conditions made it impossible to carry out DSC analyses to characterise the materials further. On the other hand, it did not represent a problem for the TGA campaign (as discussed in the conclusions of Section 5.1).

Other campaigns have been completed in the same laboratory, demonstrating the reliability of the facility and contributing to the pre-existing knowledge that this project was able to benefit from [1, 11].







(b) Balance and radiation shields.

Figure 2.6: STA facility available at VKI: NETZSCH STA 449 F3 Jupiter® apparatus positioned inside the glovebox.

# Chapter 3

# Kinetic modelling of pyrolysis

This chapter formalises the kinetic description adopted in this thesis to reconstruct non-isothermal TGA/DTGA signals of cork/phenolic ablators. The aim is to identify reaction mechanisms that allow for the simulation of pyrolysis through a calibrated set of kinetic parameters, suitable as input for numerical solvers. Two families of mechanisms are presented: (i) multi-component (devolatilisation) mechanisms, with parallel reactions where multiple pseudo-components decompose independently; and (ii) competitive mechanisms, where multiple pathways (branches) consume a common reactant.

Competitive mechanisms, and their switching pathways, are essential to describe the temperature and heating rate dependent behaviour of the studied materials [28, 33–35], as it was described in Section 2.1.3.

### 3.1 Multi-component mechanisms

In multi-component (also referenced as parallel or devolatilisation) mechanisms, the virgin solid  $\mathcal{S}$  is represented as the sum of  $N_p$  phases  $P_i$ , as in Figure 3.1, each optionally partitioned into sub-phases  $p_{i,j}$  that degrade independently of one another [36].

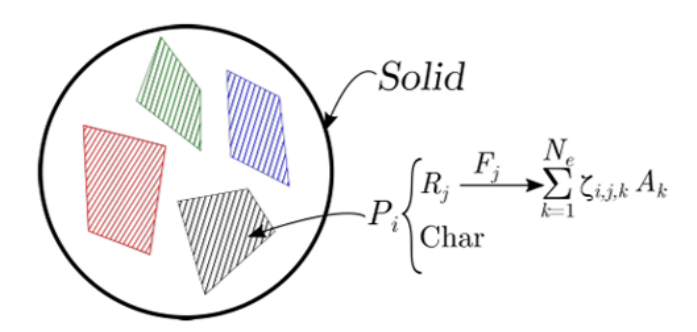


Figure 3.1: Schematic of a virgin solid and its phases in a multi-component mechanism [1].

The decomposition of  $p_{i,j}$  releases a gaseous mixture  $A_k$  according to mass coefficients  $\zeta_{i,j,k}$  and leaves a solid residue (char). The reaction progress of  $R_{i,j}$  is described by an Arrhenius law with reaction order  $n_{i,j}$  with respect to the relevant solid-state variable, using the advancement of reaction  $\alpha_{i,j} \in [0,1]$ :

$$\frac{\mathrm{d}\alpha_{i,j}}{\mathrm{d}t} = \mathcal{A}_{i,j} \left(1 - \alpha_{i,j}\right)^{n_{i,j}} \exp\left(-\frac{\mathcal{E}_{i,j}}{RT}\right). \tag{3.1}$$

As the advancement of reaction evolves as a function of the Arrhenius parameters  $(\mathcal{A}_{i,j},\ \mathcal{E}_{i,j},\ n_{i,j})$  and temperature, the initial (virgin) density of the solid evolution is written as the sum of phase contributions,

$$\rho_{s,\mathbf{v}} = \sum_{i}^{N_p} \rho_{i,\mathbf{v}} , \qquad (3.2)$$

and the evolution of the solid density during pyrolysis is obtained from composing the density-loss contributions of each sub-phase weighted by its mass (or density) loss fraction constant,  $F_{i,j}$ : measuring the mass consumed by each reaction when  $R_{i,j}$  reaches completion  $(\alpha_{i,j} = 1)$ :

$$\rho_s(t) = \rho_{s, v} - \sum_{i}^{N_p} \sum_{j}^{N_{R_i}} \rho_{i, v} F_{i, j} \alpha_{i, j}(t) . \qquad (3.3)$$

The production rate of the gaseous products (species or elements)  $A_k$  is then expressed as:

$$\pi_{A_k}(t) = \sum_{i}^{N_p} \sum_{j}^{N_{R_i}} \rho_{i,v} F_{i,j} \zeta_{i,j,k} \frac{d\alpha_{i,j}}{dt} . \tag{3.4}$$

For convenience, the mass stoichiometric coefficients  $\zeta_{i,j,k}$  are often combined into a weighted parameter  $\tilde{F}_{i,j,k} = \zeta_{i,j,k} F_{i,j}$ , which allows the reconstruction of signals without imposing a unit-sum constraint on coefficients  $\zeta_{i,j,k}$  when a reaction produces multiple species. The key structural assumption is independence of reactions: the ODEs for  $\alpha_{i,j}$  are decoupled, and the final state (char and gas, per species or element) is fixed by the choice of  $\tilde{F}_{i,j,k}$  together with the kinetic parameters  $\mathcal{A}_{i,j}$ ,  $\mathcal{E}_{i,j}$ ,  $n_{i,j}$  [36, 37].

This formulation is widely used for carbon/phenolic ablators and effectively reproduces TGA/DTGA at a given heating rate  $\beta$ , while showing limitations in capturing pathway changes as  $\beta$  varies [1, 28].

### 3.2 Competitive mechanisms

In competitive mechanisms, the same solid reactant  $\mathcal{S}_r$  may branch into several parallel pathways,

$$\mathcal{S}_r \xrightarrow{k_i(T)} \ \zeta_i \, \mathcal{S}_i + \left(1 - \zeta_i\right) \mathcal{G}_i, \qquad i = 1, \dots, N_{\mathrm{prod}}. \tag{3.5}$$

creating solids  $\mathcal{S}_i$  and gases  $\mathcal{G}_i$  that can react further in sequence. Depending on the heating rate experienced, some pathways will be favoured over others, since the kinetic coefficient of each reaction is a function of temperature,  $k_r(T)$  in Eq. (3.6). Indeed, competition among branches reflects differences in the kinetic parameters  $(\mathcal{A}_r, \mathcal{E}_r)$  and enables pathway selection that depends on the thermal conditions [38]. The evolution of solid densities combines production terms (from parents that generate  $\mathcal{S}_i$ ) and consumption terms (from the reactions that deplete  $\mathcal{S}_i$ ):

$$\frac{\mathrm{d}\rho_s}{\mathrm{d}t} = \sum_{\mathrm{prod}} \left( \zeta_s \ k_r \ \rho_{reac}^{n_r} \right) \ - \ \sum_{\mathrm{cons}} \left( k_r \ \rho_s^{n_r} \right) \ , \qquad k_r(T) = \mathcal{A}_r \ \exp\left( -\frac{\mathcal{E}_r}{RT} \right). \tag{3.6}$$

Collecting the active solid variables in the vector  $\rho = [\rho_1, \dots, \rho_N]^T$  yields the matrix system

$$\frac{d\rho}{dt} = A(T)\,\rho. \tag{3.7}$$

where A(T) is lower triangular when only forward reactions are admitted, and becomes block-diagonal when independent material components are treated side-by-side.

This structure allows solid/gas yields and DTGA peaks to emerge from branch competition and to change with the thermal profile  $(\beta)$ , accommodating the activation of intermediates and shifts of dominant pathways observed for cork/phenolic systems [1, 28].

In operational terms for the next chapters, the multi-component scheme is a special case of the competitive formulation in which A(T) is diagonal (no competition). In that limit, reactions are decoupled and (crucially) the final residual mass/char is predefined by the constant  $F_{i,j}$  and does not change with heating rate [36, 37]. Competitive mechanisms, in contrast, render yields and DTGA peaks as emergent properties of branch selection and thus sensitive to  $\beta$  [1, 28, 33].

# Chapter 4

# Materials and methods

In the subsequent chapter, the two cork/phenolic ablators tested in this thesis are introduced. Successively, the procedures used in this experimental campaign to obtain Thermogravimetric Analysis data from their thermal degradation are presented. The post-processing of the gathered experimental data is explained in detail. The data obtained following this methodology are essential for characterising the thermal behaviour of materials. The last paragraph of this chapter describes the numerical process that produces the optimised kinetic parameters from this dataset.

### 4.1 Materials

The experimental campaign investigated two cork/phenolic ablators, each produced by a different manufacturer and delivered to VKI in the form of prefabricated boards. Since detailed formulations are often proprietary, only publicly available information is reported below.

### Cork 1

Cork 1 is an ablative material produced by Amorim Cork Solutions and commercially known as cork P50. It is derived from high-density cork granules ( $Quercus\ Suber$ ) with a particle size of 0.5–1 mm, mixed with a plasticised phenolic resin as a binder. The weight ratio is attested around 80% cork and 20% phenolic resin in literature [4]. Manufacturer data reports a density of 448-512 kg/m³ at 20°C and a thermal conductivity of 0.07 W/m/K [39].

#### Cork 2

The second material, hereafter referred to as "Cork 2", is a cork/phenolic composite supplied under confidentiality by another industrial manufacturer. Its exact formulation was not disclosed to the author. A resin-to-cork ratio close to 1:4 can be assumed, consistent with Cork 1 and other similar ablative systems [31, 40].

### 4.2 Experimental methodology

The experimental parameters of this campaign were defined accordingly to the final objective. Probably the most important of these parameters is the heating rate. The optimisation of parameters should be based on sets of data obtained from multiple heating rates  $(\beta)$ . Different  $\beta$  allow for the correct representation of the temperature and time-dependent behaviour of the porous materials studied [33]. Heating rates were selected at 5, 20 and 40 K/min (considering a linear temperature increase), allowing for comparison with past TGA campaigns conducted at the Institute.

The maximum capabilities of the STA device (in the configuration described in Section 2.2) are exploited by selecting 40 K/min in the set of heating rates. At this rate, the resolution of the signal is improved at the cost of decreased sensitivity. On the other hand, a lower rate (5 K/min) results in higher accuracy. The maximum final temperature is dependent on the crucibles and the STA apparatus and was set at 1373 K. The lower temperature limit was set slightly above ambient temperature, as starting each experiment by increasing the temperature is more time-efficient. Once more, the importance of a robust numerical model is highlighted by the fact that the maximum temperature and heating rate values that can be achieved in laboratory experiments remain considerably lower than those experienced in atmospheric entry conditions.

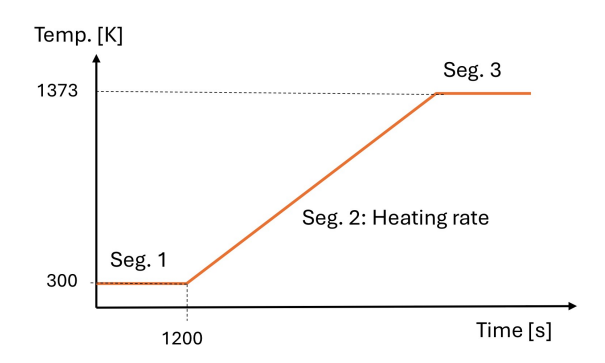


Figure 4.1: Temperature profile of dynamic TGA

A schematic of the thermogravimetric analysis temperature profile is presented in Figure 4.1. It consists of 3 segments. Segments 1 and 3 are 20-minute temperature equilibration steps (isothermal), respectively at minimum and maximum temperature. Segment 2 consists of a linear temperature increase, starting at 300 K and reaching 1373 K at the prescribed rate ( $\beta$ ). Its time duration is then dependent on the selected heating rate. Segment 3 is then followed by the cool-down of the sample to ambient temperature. During the cool-down, temperature and mass are not measured, but this stage adds to the total time required for each experimental run.

The same temperature programme is used for the blank or baseline run before each measurement. During the baseline, the values for the empty crucible (the same one used for the experiments) are measured. This run is necessary to account for the buoyancy

effect and the mass of the crucible and is subtracted from the subsequent experimental results.

Additional factors to finalise the experiment's configuration are to be considered. Crucibles, for example, can be made of different materials, depending on experimental temperatures and samples (crucible material must not interact with the sample).

For this campaign, alumina  $(Al_2O_3)$  crucibles with a cylindrical shape of approximately 5 mm diameter and 3 mm height were selected and used without a lid. In the literature about TGA experiments aimed at identifying kinetic parameters, the open lid approach is usually preferred, as it lessens secondary reactions. On the contrary, DSC measurement would have required platinum crucibles and a pierced lid [30, 41].

The presence of a lid increases the residence time of pyrolysis gases and the pressure. There's no evidence about which configuration better resembles an ablator in flight conditions. It is possible that a pierced lid could better represent the longer residence time of pyrolysis gases, characteristic of deeper zones of the heat shields [37].

During the experiments, the TGA is purged with an inert gas (Argon) to ensure a constant atmosphere, a reduced residence time of pyrolysis gases and a uniform heat transfer inside the furnace. Argon was used as a purge (50 ml/min) and protective (20 ml/min) gas for all the segments of the TGA experiment. A protective gas flow of Argon at 100 ml/min was set during cool down, at the end of the final isothermal segment. The same conditions were maintained during the calibration phase and baseline runs.

At VKI, an established practice has been developed over the years for campaigns involving STA experiments. Once the experimental parameters have been defined, a temperature calibration is the first stage of each campaign. This procedure relies on the measurement of high-purity metals (>99.99%) in accordance with the protocol instructed by the instrument manual. In the present campaign, four reference metals (Sn, In, Al and Zn) were employed. Their purity enables the identification of their experimental melting points with the metals' phase-transition temperatures. For each metal, approximately 8 mg were subjected to two consecutive heating—cooling cycles with a maximum temperature above their melting point. The registered transition temperatures were then compared to theoretical values. It is necessary to repeat the illustrated calibration procedure for all the heating rates intended for investigation during the campaign. The resulting calibration curves are stored in the instrument software and applied, for the corresponding heating rate, to correct the temperature values of all the subsequent measurements [11, 41].

Table 4.1 lists all the experimental runs whose results were relevant to this study. The run Cork2\_20K\_02 was discarded, as the absence of purge gas flow during the setup invalidated the measurement. Compared to previous campaigns, the balance required longer settling times; hence, the gas flow was temporarily turned off to assess the persistent mass decrease observed at ambient temperature. The purge gases were eventually excluded as the cause of this anomaly, which was later identified thanks to Cork2\_40K\_04.

The relevance of Cork2\_40K\_04 lies in the fact that the glovebox enclosing the Netzsch analyser was sealed and the controlled atmosphere re-established. This configuration enabled the verification of two key assumptions in this work: first, that operating the TGA outside a controlled atmosphere does not significantly affect the results; and second, the identification of the initial mass loss observed in Cork 2 samples as moisture volatilisation. The analysis of these two hypotheses is discussed in Paragraph 5.1, where results are presented.

Table 4.1: Relevant samples tested during this campaign. Each sample run is associated with a code that specifies material, heating rate and repetition.

Heating rate $(\beta)$	Code			
	Cork1_5K_01			
5 K/min	Cork1_5K_02			
	Cork2_5K_01			
	Cork2_5K_02			
	Cork1_20K_01			
	Cork1_20K_02			
$20~\mathrm{K/min}$	Cork1_20K_03			
	Cork2_20K_01			
	Cork2_20K_03			
	Cork2_20K_04			
	Cork1_40K_01			
	Cork1_40K_02			
$40~\mathrm{K/min}$	Cork1_40K_03			
TO IX/IIIII	Cork2_40K_01			
	Cork2_40K_02			
	Cork2_40K_03			
30 K/min	Cork2_30K_01			
$1h  ext{ isothermal} + 40  ext{ K/min}$	Cork2_40K_04			

A further outcome was the considerable reduction of the balance settling time once the controlled atmosphere was restored, which confirmed that the mass oscillations previously observed were caused by the open glovebox.

Finally, the test with  $\beta=30~\mathrm{K/min}$  (Cork2\_30K\_01) was performed to investigate a small anomaly at 600 K: a hollow in the mass loss curve of Cork 2 runs at 40 K/min. Ideally, the possible evolution of this feature and the associated DTGA spikes should have been examined at a higher heating rate, but this was not achievable due to instrument limitations. Therefore, an intermediate rate was selected to improve the understanding of this phenomenon.

#### 4.2.1 Sample production

The preparation of the samples is crucial to ensure reproducibility and comparability of the thermogravimetric analyses. Torres-Herrador highlighted two key sample characteristics that affect thermal analysis: an improved contact surface between sample and crucible and a sufficient sample mass [2, 37].

Both requirements are met by powdering and compressing the material, although this inevitably destroys the native microstructure and nullifies its potential influence on the measured kinetics. The minimum sample mass must be selected together with the experimental heating rate to guarantee acceptable internal temperature gradients. For low-density porous materials (carbon/phenolic ablators and cork biomass), it is therefore common to powder and compress specimens before STA testing to achieve a sufficient sample mass [16, 18, 21, 37]. Based on the VKI know-how, a target mass of 25 mg was designated for cork/phenolic samples. Poor contact between sample and crucible remains more critical for DSC.

Perin [11] proved that inclusion of sandpaper during grinding had a negligible influence on TGA results. Nevertheless, a metal grinder was used to grind the material in this campaign, reducing potential contamination from abrasive residues. A custom metallic mould (Figure 4.3) was manufactured by VKI technicians to produce cylindrical specimens, allowing for a shape consistently compatible with the STA crucibles (5-6 mm diameter, 3-4 mm height). The powder was compacted by inserting the mould in a manual hydraulic press. Compacted cylinders were then gently extracted and stored in clean glass vials to avoid moisture uptake.



Figure 4.2: Cork 2 board slice and corresponding ground powder used for sample preparation. Powdering combined with compression allows for higher sample mass and improved contact with the crucible.

The following routine was developed for the sample production during this campaign:

- 1. Clean tools and mould to avoid cross-contamination.
- 2. Grind powder from the cork/phenolic board using a metal grinder (performed once per material batch). Figure 4.2.
- 3. Tare the balance with the empty mould.
- 4. Fill the mould and clean its outer border to avoid measuring excess material. Figure 4.3
- 5. Measure mass on the balance. Target:  $m \approx 25 \pm 1 \,\mathrm{mg}$ .
- 6. Press the powder at  $\approx 15$  kN using the hydraulic press.
- 7. Extract the cylindrical sample and store it in a glass vial. Figure 4.4a
- 8. Clean the mould and repeat (skip step 2 after the first powder production).

A total of eighteen samples were produced for each material. Individual masses were recorded and used to compute the mean and standard deviation reported in Table 4.2. By using the developed production procedure, a low dispersion was achieved.



Figure 4.3: Open mould containing powder before the pressing.

Table 4.2: Average and standard deviation of sample masses for each cork material.

Material	Mean mass [mg]	Standard deviation [mg]
Cork 1	25.43	0.62
Cork 2	25.54	0.79

Figure 4.4a shows the final Cork 2 specimens stored in glass vials. Cork 2 exhibited higher cohesion and lower bulk volume at equal mass compared to Cork 1, which tended to be more friable.

Figure 4.4b compares a virgin Cork 1 sample to charred samples after a TGA experiment. The charred specimens show clear shrinkage and mass loss, consistent with charring and volatilisation during pyrolysis (see Section 2.1).

Produced samples were stored in dark, dry conditions at room temperature to minimise moisture uptake owing to the hydrophilic nature of cork/phenolic materials. The importance of controlled storage is illustrated by sample Cork2\_40K\_04 in Figure 5.10, whose vial was kept for several days under an inert atmosphere inside a glovebox. In this campaign, Cork 1 samples trapped less water than Cork 2 (Section 5.1); this may reflect different prior storage histories of the bulk boards or minor differences in surface porosity.



(a) Compressed Cork 2 samples stored in glass vials immediately after pressing.



(b) Virgin (brown-ish) and charred (black) post-TGA Cork 1 samples.

Figure 4.4: Shrinkage and mass loss following pyrolysis are made evident by the comparison between virgin and charred samples.

Figure 4.5 illustrates the preparation of a TGA run, following the baseline run, inside a sealed glovebox. The sample is withdrawn from the glass vial where it was stored and positioned inside the alumina crucible. A gentle pressure is applied to improve contact between sample and crucible, Figure 4.5a. Then the crucible is positioned on the balance (Figure 4.5b) before closing the furnace, initiating the purge gas flow and launching the temperature programme and the associated TGA.



(a) Pressing of the sample disc inside the crucible to improve the contact surface.



(b) Positioning of alumina crucible on the balance.

Figure 4.5: Setup of an experimental run. The sample is positioned into the crucible, which is then centred in the crucible-holder slot on the balance.

#### 4.2.2 Post-processing of the experimental data

Below, the workflow utilised to convert the Netzsch STA output files (TXT) into analysis-ready CSV files is summarised. The parser included in *Pyropy* reads the TXT files after skipping the instrument header lines. The relevant information is imported from the columns corresponding to temperature [°C], time [min], mass [%], and segment identifier. TGA output files (TXT) also include columns for gas flow, DSC signal and sensitivity. The file header that precedes these data columns also coantains information about campaign, material, temperature programme, sample mass and other useful information about the specific run. Data are then converted to standard units (temperature to Kelvin, time to seconds). Optional segment selection can be applied, and the experiment clock is re-zeroed at the first retained sample.

Before computing the derivative, the mass signal is smoothed to reduce random fluctuations that would otherwise be amplified by numerical differentiation. This ensures that the computed mass-loss rate is not affected by high-frequency noise introduced by

the instrument or acquisition process. A Savitzky–Golay (SG) filter, in this case with a polynomial order of 2 and a window length of 50 points, is applied to the mass vector to attenuate noise. The smoothed mass is then normalised such that the first point of Segment 2  $(m_0)$  corresponds to 100% (i.e.,  $m/m_0 \times 100$ ). Normalisation mitigates baseline offsets, enables direct comparison between tests, and provides a physically interpretable range.

The mass-loss rate is obtained as a temperature-based derivative using a chain-rule formulation that is robust to small temperature oscillations:

$$\frac{dm}{dT} = -\frac{dm/dt}{\beta} \tag{4.1}$$

where  $\beta$  is the programmed heating rate expressed in K/s. The time derivative dm/dt is computed by finite differences, using central differences for interior points and forward/backward schemes at the boundaries.

A second, milder SG filter (order 2, window length 31) is applied to the obtained massloss rate curve. The negative sign ensures that dm/dt remains positive during mass loss, consistent with standard TGA rate conventions for representation.

The reading, computing and storing procedure was implemented in a new Python script added to *Pyropy*, that will be introduced in Section 4.3. Each one of the resulting CSV files contains one row per time sample with the following columns:

- index [-]: 0-based row counter
- time [s]: experiment time, re-zeroed
- temperature [K]: measured temperature
- mass [%]: normalised mass  $(m/m_0 \times 100)$
- derivative [%/K]: mass-loss rate (dm/dT)
- **segment** [–]: segment identifier of temperature programme

These files are subsequently averaged (as described in the following section) and used as inputs for the parameter optimisation procedure.

#### Average and standard deviation

From the post-processed data collected in the CSV files, the average and standard deviation were computed. The average of different runs (at the same  $\beta$ ) provides trustworthy inputs for the fitting of kinetic parameters. Standard deviation is used to confirm repeatability.

For each heating rate, the post-processed thermogravimetric signals from all repetitions were restricted to a common temperature interval and corrected to ensure a strictly monotonic mass loss profile (this was not the case for  $\beta = 5$  K/min due to the high number of measurements at similar temperatures). The signals were then re-sampled on a

uniform temperature grid by cubic spline interpolation (with zero smoothing), which enabled a pointwise calculation of average and standard deviation on temperature. The averaged mass loss rate was then calculated by derivation of the obtained averaged mass loss curves.

Also for the averaged values, Cork 1 was normalised to 100% at its first recorded sample mass value, while for Cork 2, mass was normalised after water evaporation was completed, at 420 K. Later, the water-evaporation segment was completely excluded as it was not of interest for the kinetic parameters optimisation that is based on the obtained averaged curves.

At each temperature node  $T_j$  across the N experimental runs (N=3 for 40 and 20 K/min, N=2 for 5 K/min), we computed the arithmetic mean and the standard deviation of the quantity x (mass fraction m or mass-loss rate dm/dt) as

$$\overline{x}(T_j) = \frac{1}{N} \sum_{i=1}^{N} x_i(T_j) \quad ,$$
 (4.2)

$$\sigma_x(T_j) = \sqrt{\frac{1}{N} \sum_{i=1}^{N} (x_i(T_j) - \overline{x}(T_j))^2}$$
 (4.3)

The standard deviation is calculated as the square root of the average squared deviations from the mean. To mitigate noise in the values of the mass-loss rate, an SG filter (80-point window, third order) was applied to both the averaged curve and the corresponding standard-deviation profile. The time axis was reconstructed from the corresponding heating rate and the imposed temperature grid.

#### 4.3 Arrhenius parameters optimisation: Pyropy

Pyropy [42] is a Python package developed by Torres-Herrador across his Master's thesis, Research Master project and PhD. thesis experiences at VKI [1, 2, 30]. It was conceived as the evolution (in Python) of two earlier parameter identification tools: the in-house FiTGA (Fitting TGA Algorithm) code<sup>1</sup> and the property–estimation library embedded in Gpyro<sup>2</sup>. Pyropy retains FiTGA's emphasis on curve reconstruction and objective minimisation while including the capability of working on the competitive–kinetics formalism with robust global search strategies (Shuffled Complex Evolution (SCE) algorithm) that proved effective in Gpyro.

In this Section, inputs—outputs, curve reconstruction, the objective function, and the SCE algorithm developed at the University of Arizona (SCE-UA) optimiser are discussed in this order. The same optimisation procedure is used for both the parallel and the competitive mechanisms already introduced in Sections 3.1 and 3.2. Differences

<sup>&</sup>lt;sup>1</sup>Implemented in Matlab; multiple optimisers (nonlinear least squares, GA, hybrid GA+LSQ) were available [2].

<sup>&</sup>lt;sup>2</sup>Gpyro features a parameter–estimation module built around the competitive–reactions scheme and implements GA and SCE variants [30].

arise in how the model is assembled from the reaction scheme template and in the PyrolysisModel operated.

#### Inputs.

- Experimental data: a CSV file for each heating rate, containing TGA/DTGA averages (Section 4.2.2); providing time t, temperature T, solid density  $\rho$  and its numerical derivative  $d\rho/dT$ . When mass fraction is mentioned, it is defined once as  $m(T) = \rho(T)/\rho_0$ .
- Pyrolysis model: specifies which variant (parallel or competitive) will be used to read and optimise kinetic parameters.
- Reaction scheme template: a JSON template defines the reaction network and establishes the set of unknown parameters to be calibrated.
- Boundaries (and optional initial guesses): lower/upper limits for each parameter that define the range for the initial sampling of the population. Note that for the pre-exponential factor the range is imposed on the decimal logarithm of the pre-exponential, A ( $A = \log_{10}(\mathcal{A})$ ).
- Optimisation settings: SCE-UA population size, number of complexes, evolution/shuffle loops and stopping tolerances.
- Iterations and repetitions: Iterations are independent restarts of SCE optimisation campaigns. Repetitions  $(N_{rep})$  cap the number of saved function evaluations (a full simulate-and-score per one parameter set) as a stopping limit of an SCE optimisation campaign.

#### Outputs.

- A CSV summary with the best parameter set and its associated objective function value
- A JSON file where the template placeholders (unknowns) are replaced by the optimised parameters (best set).

As a result, the optimisation returns the best set of Arrhenius parameters for the chosen scheme. For the multi-component model, reaction i: activation energy  $\mathcal{E}_i$ , logarithmic pre-exponential  $\mathbf{A}_i = \log_{10}(\mathcal{A}_i)$ , reaction order  $n_i$ , and mass-loss fraction  $F_i$ . For the competitive model, rection branch i:  $\mathcal{E}_i$ ,  $\mathbf{A}_i = \log_{10}(\mathcal{A}_i)$ , and the solid yield fraction (or mass coefficient)  $\gamma_i$ .

#### Curve reconstruction

For each parameter set proposed by the optimiser, Pyropy builds the time-temperature profile at defined heating rates and reconstructs the mass loss curve,  $\rho(T)$  and its derivative  $d\rho/dT$ . For linear temperature ramps:

$$T(t) = T_0 + \beta \cdot t, \qquad \beta = \text{const. [K/s]} \ . \eqno(4.4)$$

Depending on the reaction scheme and the pyrolysis model provided, the parameter set differs. Multi-component and competitive mechanisms lead to the solution of different systems to obtain the simulation of the TGA curve.

Multi-component (parallel) model. When reconstructing density loss curves for a parallel reaction scheme (Section 3.1), the degradation is expressed with independent nth-order relations:

$$\frac{d\alpha_i}{dt} = k_i(T) \left(1 - \alpha_i\right)^{n_i}, \quad k_i(T) = \mathcal{A}_i \exp\left(-\frac{\mathcal{E}_i}{RT}\right) \ . \tag{4.5}$$

The advancement of the *i*-th reaction  $(\alpha_i(t))$  is the state variable. The corresponding reaction has not started yet when  $\alpha_i = 0$  and is completed for  $\alpha_i = 1$ . This parameter can be related to the density evolution by the following equation [2]

$$\rho(T) = \rho_0 \left[ 1 - \sum_{i=1}^{N_r} F_i \ \alpha_i(T) \right] \tag{4.6}$$

where  $N_r$  is the number of independent reactions of the proposed model, with  $i=1,\ldots,N_r$  and the advancement of reaction is scaled by the fraction density loss  $F_i$ . This constant expresses the fraction of density that is lost when reaction  $R_i$  reaches completion (i.e.  $\alpha_i=1$ ) [1]. The four kinetic parameters that describe each reaction  $R_i$  are then identified: activation energy  $\mathcal{E}_i$ , pre-exponential factor  $\mathcal{A}_i$ , reaction order  $n_i$  and  $F_i$ .

Competitive model. When working on competitive reaction schemes (Section 3.2), the solution of an ODE system is required to reconstruct the  $\rho(T)$  curve. The vector  $\mathbf{z}(t)$  contains the density values of reactants and products. Under matrix formalism, the system that needs to be solved is:

$$\dot{\mathbf{z}} = \mathbf{A} \ \mathbf{z} \tag{4.7}$$

Dependent variables (all gaseous products and solid products that do not further react) are removed, and the unknown gas yields are assumed equal to  $1-\gamma_i$ ; so that A is square and full rank and z(t) contains only the solid-species densities. Excluding backward reactions (not observed in practice for the highly dissipative and irreversible reactions of pyrolysis), A can be arranged lower-triangular, which improves numerical treatment [1].

The elements  $a_{x,y}$  of matrix A(T) represent the production and consumption of all solid species through each *i*-th reaction as a function of kinetic rate  $k_i(T)$  and solid yield fraction  $\gamma_i$ . Thus, identifying a set of three Arrhenius parameters for each reaction  $R_i$ :  $\mathcal{E}_i$ ,  $\mathcal{A}_i$  and  $\gamma_i$ .

In practice, the ODEs are integrated with an initial value problem solver. The high variability and elevated values of the pre-exponential parameter ( $10^{\text{A}}$ ) attribute to this system a high stiffness. For this reason, the Radau method is selected. Additionally, the solver was fine-tuned during this project to pass A(T) as the explicit Jacobian  $J(T) \equiv A(T)$  to enhance stability, preventing overflow errors, and efficiency.

#### Evaluation by objective function value

Each candidate parameter vector p (for a 2-reaction competitive model the vector will be formed as  $\mathbf{p} = \{\mathcal{E}_i, \ \mathcal{A}_i, \ \gamma_i, \ \mathcal{E}_j, \ \mathcal{A}_j, \ \gamma_j\}$ ) is scored by an objective function  $S(\mathbf{p})$  (Eq. (4.8)) that measures the mismatch between model predictions and experimental observables over all heating rates, following the deterministic least-squares misfit framework described in [38].

Concretely, the outputs d(p) (a vector of simulation results for p at variable values of time and temperature from experiments) and the observations  $d^{obs}$  are compared considering a weighted least-squares norm ( $\|\cdot\|_W$ , W is the weighting matrix) as the measure of their mismatch

$$S(\mathbf{p}) = \frac{1}{2} \| \mathbf{d}(\mathbf{p}) - \mathbf{d}^{\text{obs}} \|_{\mathbf{w}}^{2}$$
 (4.8)

Therefore, the best set of parameters  $p_{best}$  is the solution (among the admissible solutions  $\mathcal{P}_{ad}$ ) that minimizes the following misfit function

$$p_{\text{best}} = \arg\min_{\mathbf{p} \in \mathcal{P}_{\text{ad}}} S(\mathbf{p}) \ . \tag{4.9}$$

The data vector contains both the mass-loss curve (TGA) and its derivative (DTGA), separately contributing to the objective function [43]. The sum of squared residuals on TGA and on DTGA is formed, with a constant weighting factor ( $\tau = 10000$ ) applied to the DTGA so that both parts have comparable influence on the fit

$$S = \left\| \mathbf{d}_{\text{TGA}}^{\text{sim}} - \mathbf{d}_{\text{TGA}}^{\text{obs}} \right\|_{\mathbf{I}_{n_{\text{obs}/2}}}^2 + \tau \left\| \mathbf{d}_{\text{DTGA}}^{\text{sim}} - \mathbf{d}_{\text{DTGA}}^{\text{obs}} \right\|_{\mathbf{I}_{n_{\text{obs}/2}}}^2. \tag{4.10}$$

Operationally, evaluating a candidate p means simulating the pyrolysis to obtain d(p) for all heating rates, assembling the TGA/DTGA residuals, applying the appropriate weighting, and returning the scalar score S(p) that the SCE algorithm uses to rank and refine candidates [38].

#### 4.3.1 Model calibration: Shuffled Complex Evolution algorithm

Pyropy performs bounded, derivative-free global optimisation of the kinetic parameters defined by a JSON reaction scheme so that simulated multi-rate TGA/DTGA curves match experiments. Once the curve reconstruction model and the misfit are defined, parameter search is carried out with the SCE-UA algorithm, chosen for its robustness to non-convex objectives (multiple local minima can provide satisfactory results with different combinations of kinetic parameters [43]) and noisy evaluations.

Given bounds for each parameter, SCE-UA draws an initial random population ("burn-in sampling"), evaluates each individual p once, sorting them by score, and partitions the population into groups (complexes). Within each complex, a local search is performed: multiple simplexes are repeatedly formed and evolved via reflection, expansion, contraction or randomisation to replace the worst member of the current simplex when an improved candidate is found. After evolving all complexes, the full population

is re-sorted and shuffled to exchange information for a global search. The cycle then repeats, Figure 4.6.

The optimisation is terminated on the user-set evaluation budget (repetitions) and/or when population spread and best-value improvement fall below tolerances. By iterations, we denote independent restarts of SCE-UA, and repetitions denote the number of saved function evaluations  $N_{rep}$  (each is one full simulate-and-score of a parameter set), consistent with the inputs listed above.

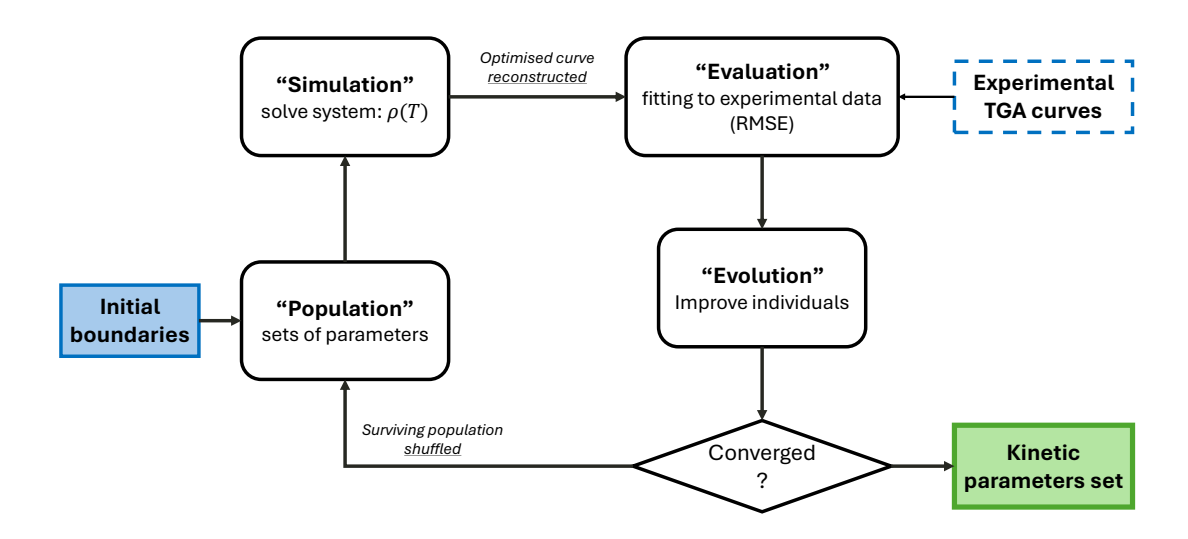


Figure 4.6: Basic structure of the optimisation loop.

## Chapter 5

# Results and discussion

#### 5.1 Experimental TGA results

Results are presented after normalisation and smoothed as explained in Section 4.2.2. The first value registered in Segment 2 (temperature ramp) represents 100% of the virgin sample mass. This accounts for the slight oscillation of the scale during Segment 1. This results in an apparent reduction of mass at constant room temperature. The repeatability and validity of the experiments were not compromised. It is possible to identify the cause in the non-controlled atmosphere in which the experiments were conducted. Old data for previous experimental campaigns conducted at VKI on Cork 1 were available. Nonetheless, new experiments were run to ensure consistency of results for the comparison with Cork 2.

Remarkable agreement between all Cork 1 results is already evident from Figure 5.1. This data visualisation is very similar to how the raw data are presented directly by the facility's software. The different steepness of mass loss curves at different  $\beta$  is due to the total running time of experiments. This doesn't imply that the evolution is identical at all heating rates. As will be discussed later on in this Chapter.

Cork 2 samples showed similar, excellent repeatability (Figure 5.2). This material was tested at VKI for the first time, and these results were satisfactory. Unfortunately, no data on TGA for Cork 2 is publicly available for comparison, underlining the importance of this experimental campaign. From these initial visualisations of data, some differences from the Cork 1 can be noted already:

- For each heating rate tested, Cork 2 presents a higher char yield
- Cork 2 evolution is clearly divided into two main phases at different inclinations. Compared to the less defined three slopes of Cork 1
- An additional phase can be clearly identified around 375 K for Cork 2

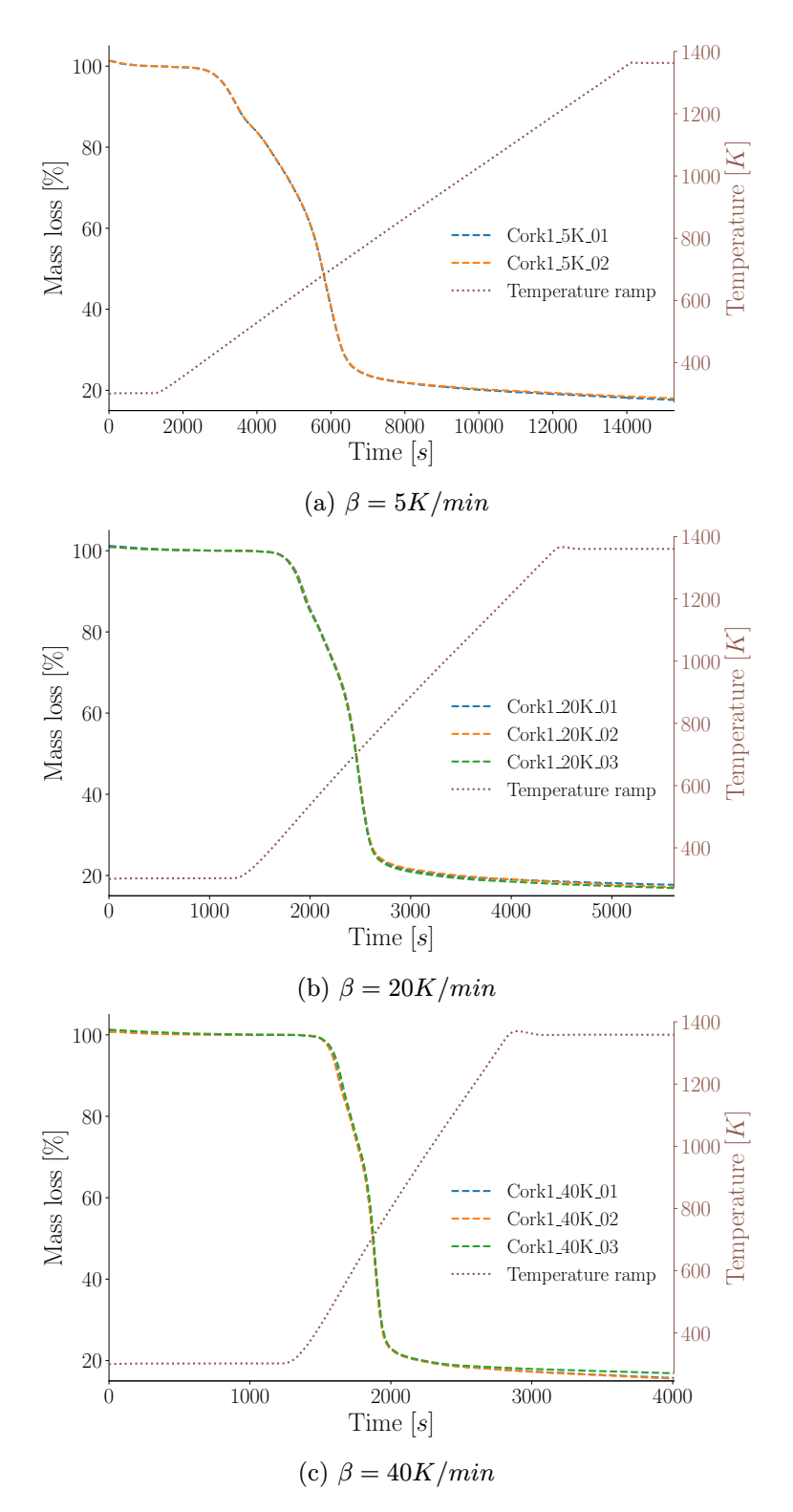


Figure 5.1: Experimental TGA data of Cork 1.

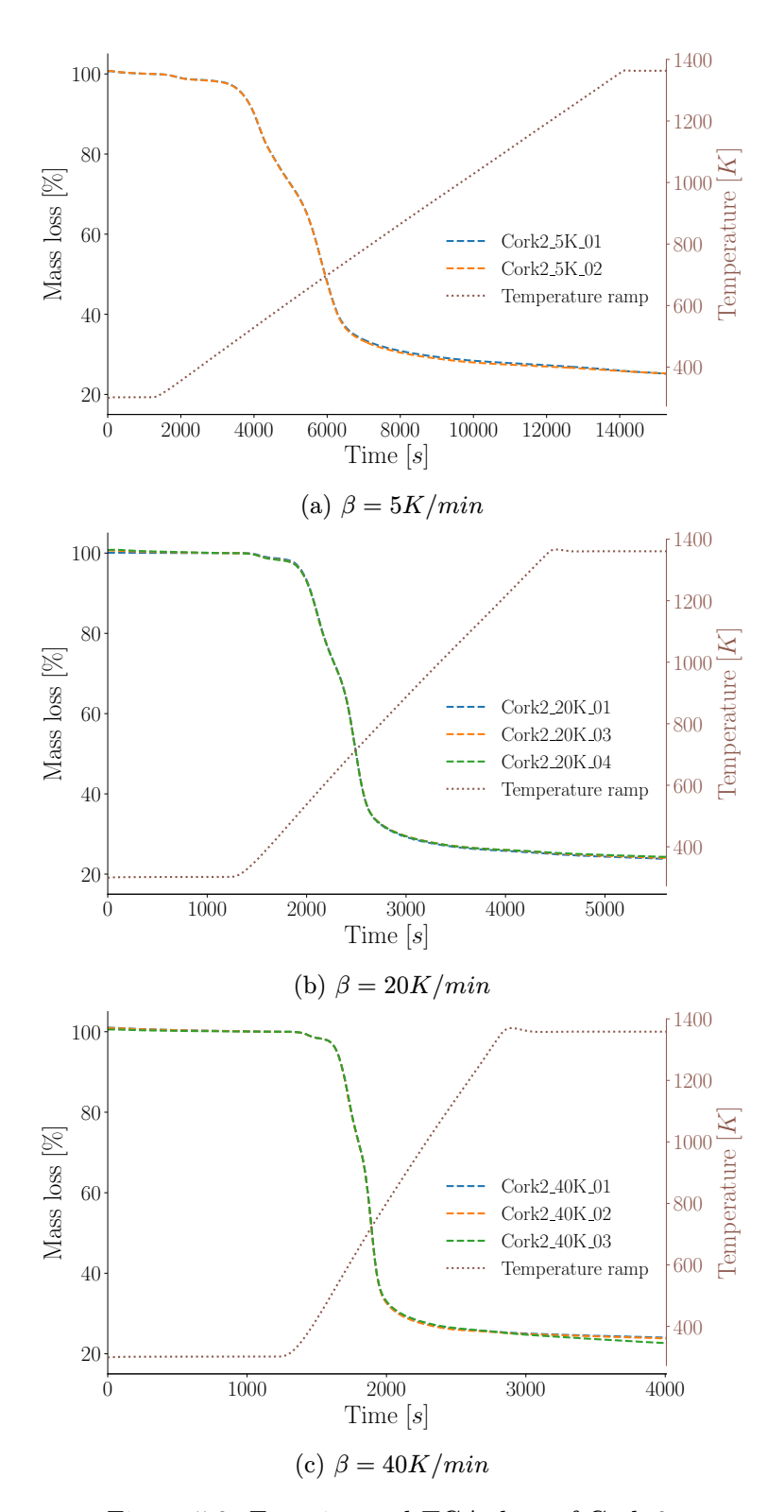


Figure 5.2: Experimental TGA data of Cork 2.

The type of visualisation adopted in this section, for the relatively short total duration of the 40 K/min runs, does not make evident the "hollow" that motivated the 30 K/min experiment. However, the anomaly is evident from the unusual spikes during the first DTGA peak in Figure 5.4c. For completeness, the additional experimental run is reported in Figure 5.5.

It is possible to see slightly better accuracy for lower  $\beta$  values, as expected [29]. This is reflected in results that are more repeatable and similar, allowing for the reduction of experimental runs. However, the difference in final mass between the three samples is never over 1.4% of the total mass, even at the highest heating rate tested ( $\beta = 40 \text{ K/min}$ ). Thus, a totally negligible discrepancy that doesn't impact the use of the data.

The numerical derivative of TGA curves (DTGA, Paragraph 4.2) presented in Figures 5.3 and 5.4, shows the reaction rates and their evolution during thermal degradation. First of all, it is possible to notice a difference in the shape and position of peaks between Cork 1 and 2. Cork 1 main reaction is characterised by higher intensity, maxing out at slightly lower temperatures. DTGA results are extremely noisy at lower heating rates. This is due to the higher number of measurements taken at each degree by an extremely sensitive scale. Starting and final spikes are to be ignored since they correspond to segments 1 and 3 of the dynamic TGA. Indeed, these are the two segments characterised by a constant temperature and will be ignored for later data visualisations.

The inflexions in the derivative of TGA data (Figures 5.3, 5.4 and 5.7) can be associated with occurring reactions, facilitating their identification and the understanding of the pyrolysis phenomena occurring. Cork 1 pyrolysis starts around 400 K and is completed before reaching 900 K at a mass of approximately 22% of the virgin sample mass (Figure 5.7a). Overlapping between the first (400 K to 500 K) and the major (650 K to 800 K) reaction, a third, lower intensity, reaction can be identified around approximately 600 K. These new results are in good agreement with the ones obtained by Sakraker [5] for the same material from a different production batch. A study by Smith et al. [32] on a cork-based composite also presents a very similar reaction pattern. This cork/phenolic ablator is produced by the same company that produces Cork 1 and differs from it in cork to resin mass ratio and granule dimensions [44].

On the other hand, Cork 2 evolution (Figure 5.7b) is interestingly different. Mass starts to evolve earlier ( $\approx 1.5\%$  loss) due to moisture volatilisation until 420 K, as it was proven in the following dedicated subsection. The first pyrolysis reaction starts later (450 K) than what was measured for Cork 1, but through a broader range of temperatures ending well after 600 K. The major reaction reaches maximum intensity between 680 K and 720 K, depending on the heating rate. Due to the delayed start of the first reaction in Cork 2, the temperature gap between the two main phases is reduced. No "intermediate" reaction takes place, in opposition to Cork 1 behaviour.

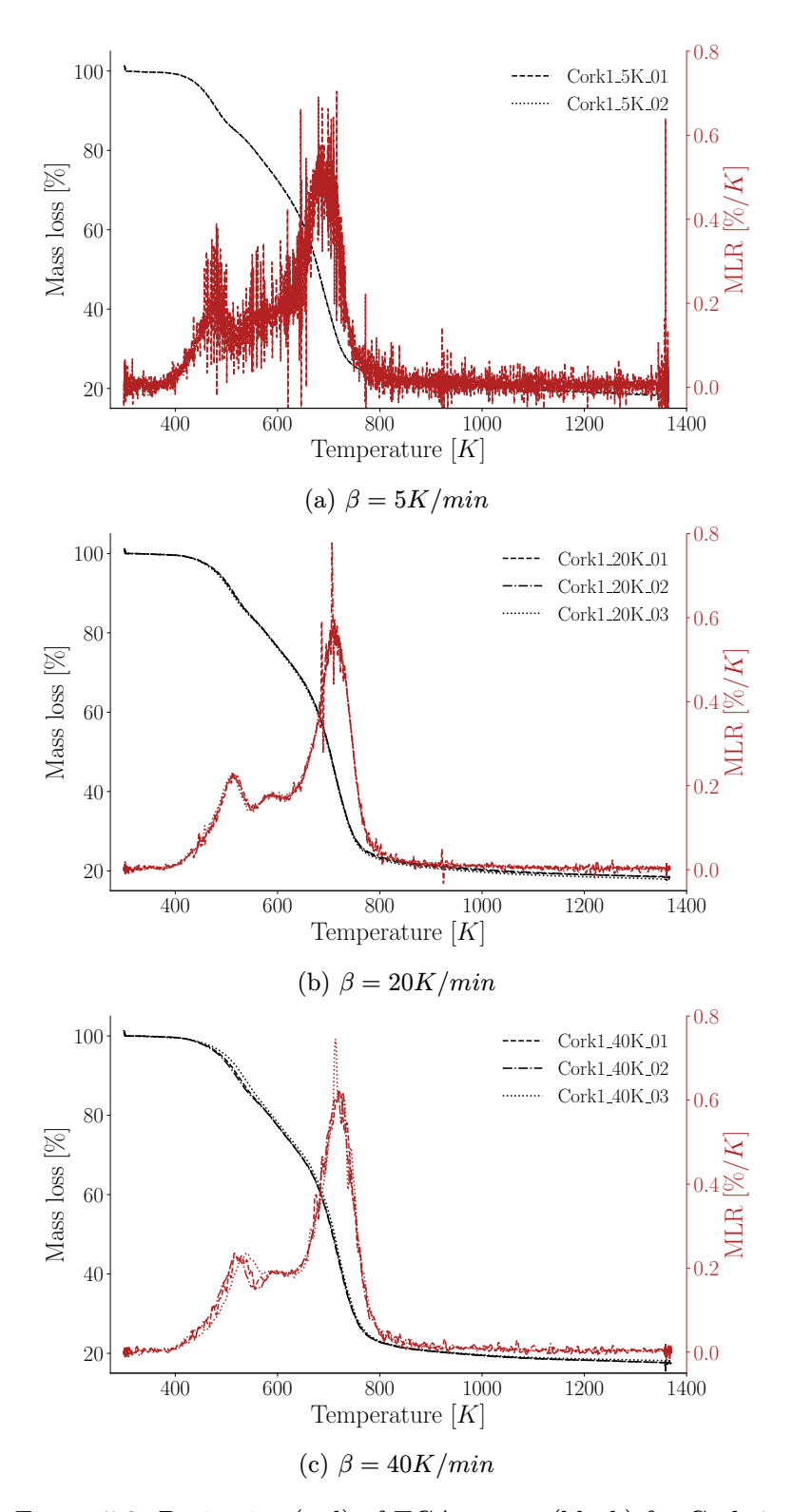


Figure 5.3: Derivative (red) of TGA curves (black) for Cork 1.

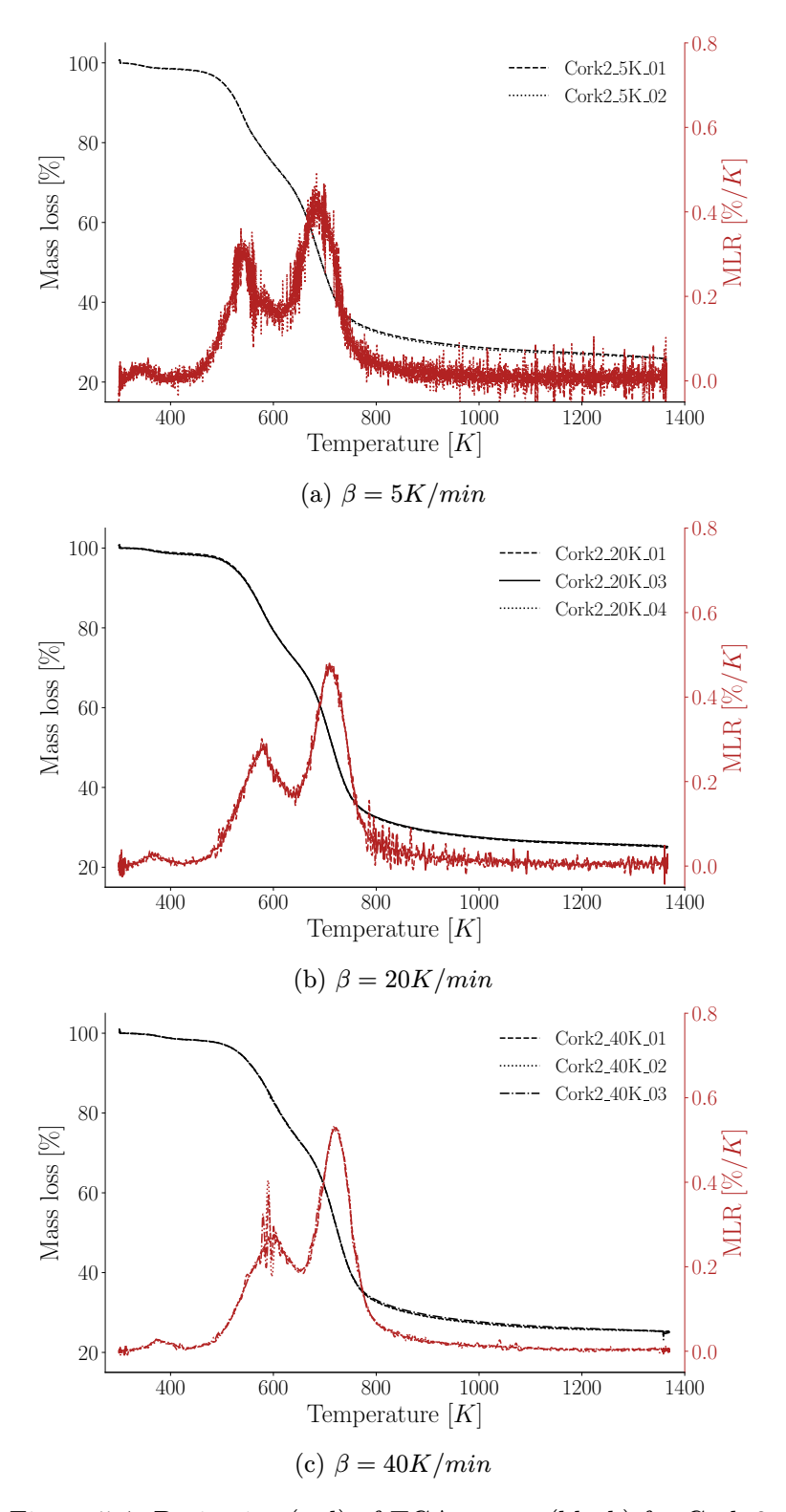


Figure 5.4: Derivative (red) of TGA curves (black) for Cork 2.

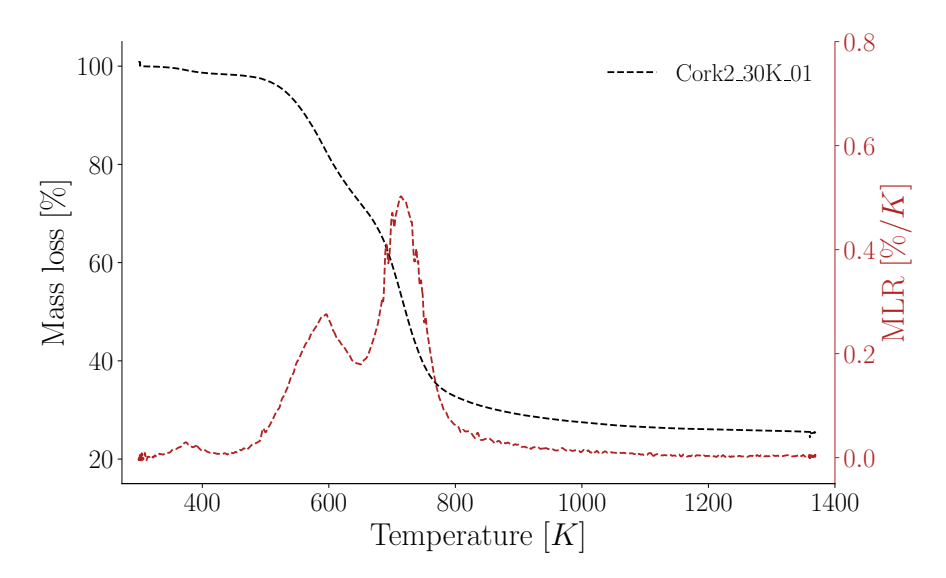


Figure 5.5: Additional experimental run for Cork 2 at  $\beta = 30K/min$ .

The association of the main peaks in DTGA curves with actual pyrolysis reactions is more complex. First of all, the exact resin mixture used is unknown for both materials. The work by Natali [16] with an epoxy-phenolic hybrid matrix demonstrates how the resin mix influences the DTGA profile of carbon-phenolic ablators, if compared to studies on ZURAM [37] or on PICA® [26]. Secondly, only the species of cork used in Cork 1 is public (i.e. *Quercus Suber*). In any case, similar behaviour is documented across various species by Şen [18]. Even if not all studies on cork powders present the same DTGA profiles [20, 21], all agree on the two-step process typical of cork pyrolysis and on the order in which the components of corks react. This sequence of reactions is analysed in great detail by Ghonjizade-Samani [17] and Şen [20].

Polysaccharides (and particularly hemicellulose, as shown by Blazquez [19]) are mainly responsible for the first reaction, approximately between 400 K and 600 K. Suberin is the main and most thermally stable component of cork and, with lignin and cellulose, contributes to the major reaction approximately at 700 K [20]. The difference between these three sub-components is in the intensity and temperature range of their degradation. Suberin evolves over a wide range of temperatures (similarly to lignin, but in two steps instead of one) while cellulose is characterised by a more intense and faster reaction.

Both materials kept losing mass after 800 K. This loss can be quantified at around 4% of mass for both Cork 1 and 2. This high temperature evolution is attributed by Bessire and Minton [25] to the third stage of phenolic pyrolysis. In PICA<sup>®</sup>, this late decomposition of phenolic resin is characterised by high molar production of  $H_2$  and high mass production of CO.

This phenomenon is also relevant for cork/phenolic ablators. Although it can not be observed in Sakraker's work [5], it is documented for cork P45 [32], for SLA-561V [22] and for a generic "aerospace cork board" [31]. Additionally, Ghonjizade-Samani [17] analyses

the same late decomposition for untreated cork powder. She proves that extractives (which include phenolic compounds) are responsible for a slight thermal instability of cork at the end of its decomposition.

In any case, the attribution of each DTGA peak to the decomposition of specific constituents is still uncertain. For example, if any epoxy resin presence was attested in the matrix mixture, its reaction would influence the gas production in the 600 K - 800 K range [16, 45]. Thus, it is not easily identifiable from TGA data only. Moreover, it is also difficult to correlate the intermediate reaction, peaking at 600 K in the pyrolysis of Cork 1, to any component's degradation. Considering that phenolic resin is more thermally stable than epoxy, it should not produce any increase in MLR at the considered temperatures. The intermediate reaction could instead be attributed to differences in the cork species or in the cork granules treatments during the production of the two ablators. Finally, a substantial difference was observed between the thermal behaviour of cork constituents lignin, cellulose and hemicellulose, when analysed as pure compounds or in cork [19]. This adds further complexity in the interpretation of the presented TGA experiments.

Figure 5.6 helps to visualise another relevant difference in the two ablators' performance: their residual mass. After pyrolysis, the char yield difference between Cork 1 and Cork 2 is consistently around 8%. From literature, it is found that cork powders under pyrolysis always decompose until losing roughly 85% of their mass [17, 19, 20] while pure phenolic resins usually lose about 46% of total mass [46, 47]. The almost complete elimination of the cork phase in composites is further proven by the X-ray tomography conducted by Foster et al. [22] on a cork/phenolic SLA, and other studies on cork powders. Therefore, the presented results of the final mass can be interpreted as caused by a difference in the cork-matrix ratio between the ablators.

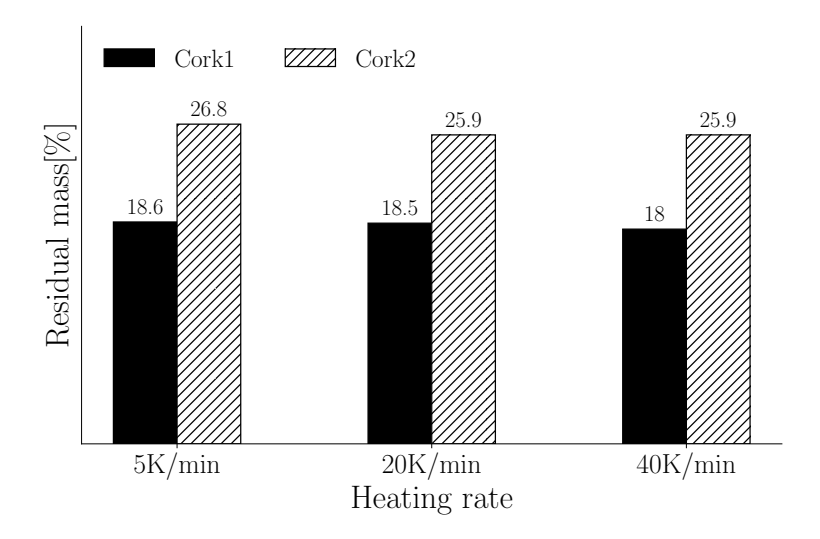


Figure 5.6: Differences in residual mass. Averaged values.

#### Heating rate dependent behaviour

Figure 5.7 is the result of the post-processing of data that was carried out as defined in Section 4.2.2. The graphs display, for each heating rate, the averaged curve and a shaded  $\pm 1\sigma$  interval which represents the standard deviation of the experimental data. The variability between low heating rate runs was expected, and the experiments are confirmed to be in excellent agreement.

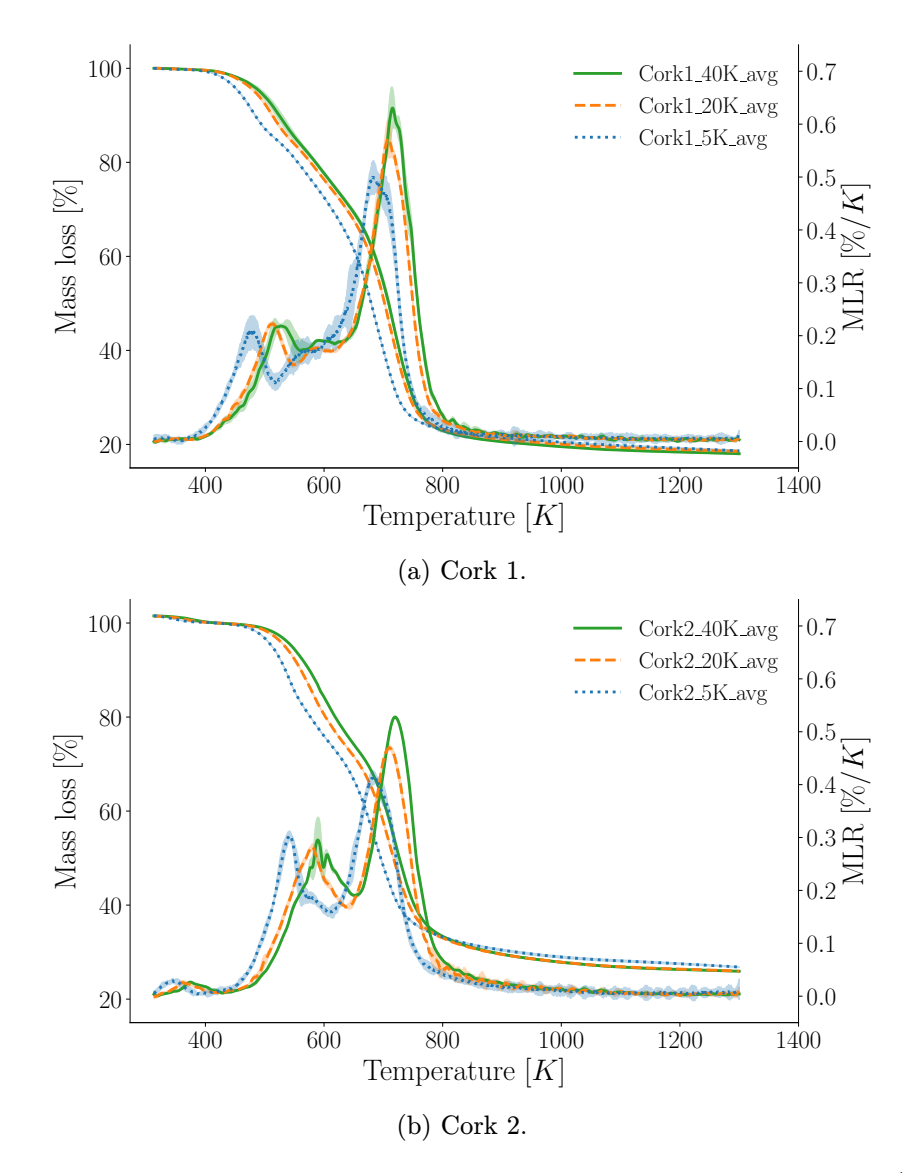


Figure 5.7: Shifting of pyrolysis reactions for different heating rates. TGA (left axis) and DTGA (right axis) curves.

The representation of averaged curves provides a clear visualisation of the shifting anticipated in Section 2.1.3. The trend observed for cork [18, 19, 21] and carbon/phenolic

ablators [11] at comparable heating rates was confirmed. An increase in the experimental  $\beta$  corresponded to a shift of the reactions towards higher temperatures. At the same time, the intensity of the second reaction was increasing. Even if no data is publicly available for higher heating rates, an inversion of this trend over 100 K/min can be foreseen, as a final confirmation of the change in the predominant paths of reaction [28].

Additionally, a decrease in the final char yield of both ablators was observed as the heating rate increased (Figure 5.6). This change is quantitatively negligible and of difficult comparison with the literature. The trend is opposite to what was recorded for *Q. cerris* by Şen [18], but Stokes reports studies with contrasting trends in phenolic resins [24].

#### Moisture volatilisation

The identification of the first reaction of Cork 2 as moisture volatilisation required further investigation. Indeed, at slightly higher temperatures, the first step of phenolic pyrolysis takes place, producing  $H_2O$  [25]. The absence of this mass loss phase in Cork 1 supported the hypothesis of trapped water evaporation, as sustained by [31, 32]. Nonetheless, an additional experiment was carried out as proof of this claim.

For Cork2\_40K\_04, the temperature programme differed from other experiments as it was specifically designed to study moisture evaporation in Cork 2 samples. It included five segments, as shown in Figure 5.8: Segment 3 consisted of a one-hour isothermal step at 80°C, introduced to ensure complete moisture removal before heating at 40 K/min in Segment 4. The temperature ramp from 27°C (after the 20-minute equilibration at ambient temperature, Segment 1) to the target of 80°C was also set at 40 K/min (Segment 2).

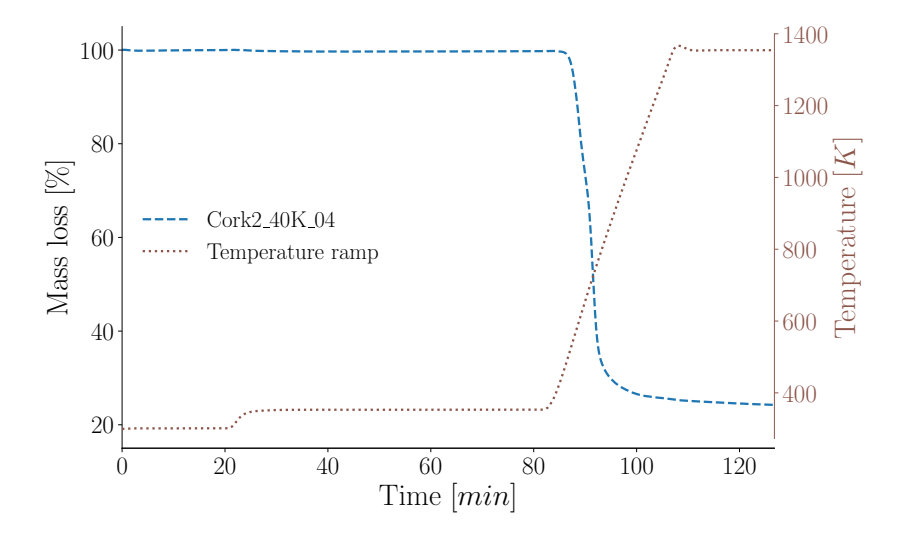


Figure 5.8: TGA curve and temperature program:  $S1=20 \text{ min at } 27^{\circ}\text{C}$ ;  $S2=40 \text{ K/min to } 80^{\circ}\text{C}$ ;  $S3=60 \text{ min isothermal at } 80^{\circ}\text{C}$ ;  $S4=40 \text{ K/min to } 1100^{\circ}\text{C}$ ; S5=20 min isothermal.

This supplementary TGA run was conducted with a sample stored under controlled atmosphere inside the sealed glovebox for several days. It is possible to see that the initial mass loss around 373 K was not recorded in this case. Also, during the isothermal phase at 80°C (Segment 3), minimal mass loss of the sample was measured (Figure 5.9).

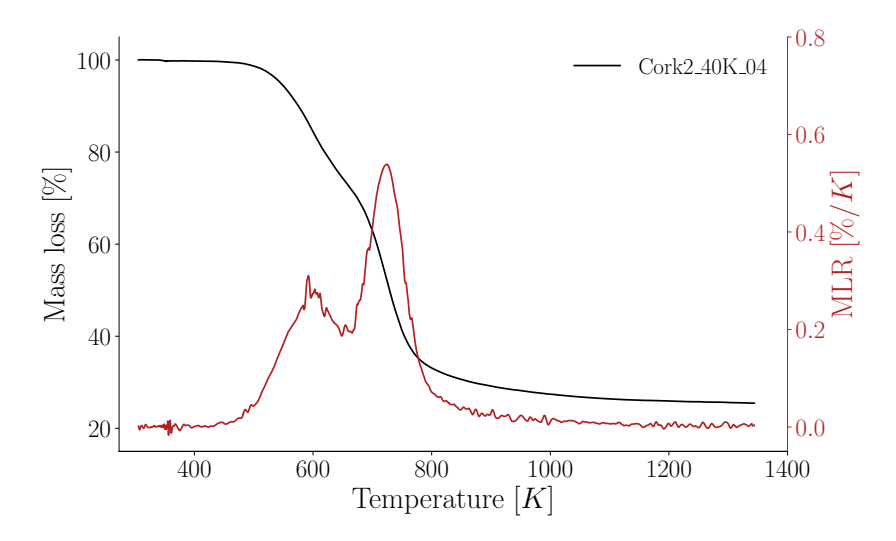


Figure 5.9: TGA and DTGA curves of Cork2\_40K\_04. Segments 2, 3 and 4.

The use of the Netzsch analyser inside a controlled atmosphere provided a valuable validation of the experimental campaign performed without a sealed glovebox. The results shown in Figure 5.10 confirm the reliability of the data collected under standard conditions, while also highlighting the advantages of carrying out TGA within a closed glovebox. Storing the samples under a controlled atmosphere for several days proved effective in eliminating residual moisture. In particular, the sample coded Cork2\_40K\_04, which was kept inside the VKI glovebox for several days, exhibited a mass loss below 1% during Segment 3 of the dynamic TGA programme, specifically designed to assess this behaviour.

Moisture absorption of porous materials is beyond the scope of this thesis. The different impact of the outgassing of absorbed  $H_2O$  on the two ablators' loss of mass is probably due to a difference in hygroscopy. A study by Wang et al. [31] on this topic for cork/phenolic ablators can be found in the bibliography. It is important to recall that the samples of both materials were reduced to powder, thereby altering their hygroscopic properties compared to the "intact bulk form" in which the ablators are used for TPS applications. The same preparation procedure was followed in both cases, and both powders were stored and tested under unconstrained atmospheric conditions.

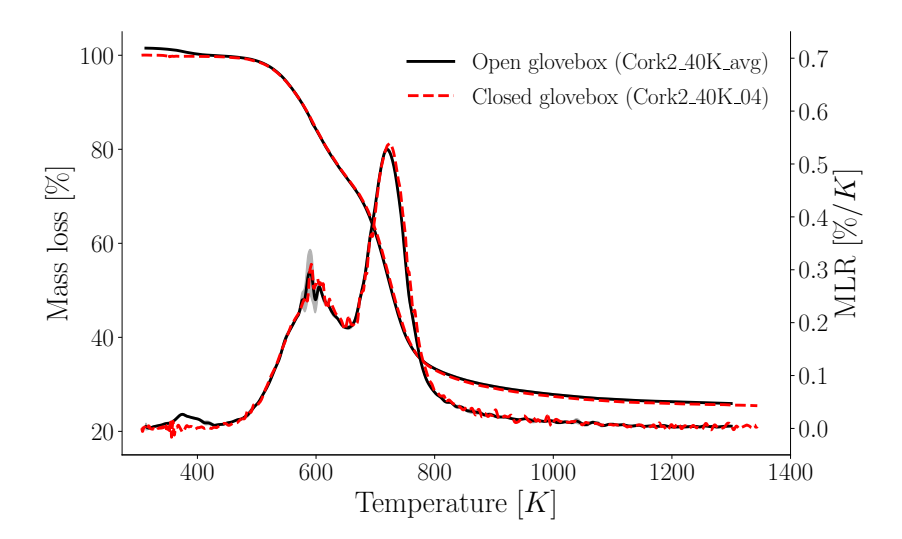


Figure 5.10: Comparison between the average of TGA experiments with open glovebox and validation experiment with closed glovebox.

#### Concluding remarks

The assumptions of this Paragraph are made thanks to the knowledge shared in the cited literature, but without knowing the exact composition and production process of the studied ablators. Indeed, it is important to always keep in mind that chemical formulation of the resin (matrix) [24] and production procedures and treatment, of both resin and cork [20], play a major role in the pyrolysis kinetics of these materials.

Higher heating rates would be valuable for future experiments, as the present dataset does not fully capture the pyrolysis process under flight-like conditions and remains limited for the optimisation of a robust numerical model. The observed shifting confirms the need for a competitive mechanism to reproduce the behaviour of these materials across different heating regimes. The observed shifting confirms the necessity for a competitive mechanism to reproduce the behaviour of these materials across different heating regimes.

The experiments demonstrated excellent repeatability of results for both ablators, enabling a robust comparison between Cork 1 and Cork 2. The analysis highlighted clear differences in reaction behaviours and residual char yield, pointing towards variations in cork-to-matrix ratios and potentially in cork species or treatments.

The additional run performed in the glovebox (Cork2\_40K\_04) demonstrated that it is possible to conduct TGA experiments without a sealed atmosphere, with reliable and consistent results. Nonetheless, the comparison confirmed the advantages of controlled storage, which reduces the effect of moisture absorption and improves the accuracy of initial mass evaluation.

This experimental campaign, therefore, established a solid foundation for the numerical analyses presented in the following chapters. At the same time, it confirmed the need for future investigations at higher heating rates to further refine the characterisation of cork/phenolic ablators.

#### 5.2 Parallel reactions model

The multi-component (parallel) formulation was assessed first than the more complex competitive mechanism, as a baseline description for the two ablators. In this mechanism, each pseudo-component decomposes independently following the nth-order Arrhenius law in Eq. (3.1), and the solid density is reconstructed by superposing the sub-phases' contributions weighted by the mass-loss fractions  $F_{i,j}$  (Eq. (3.3)).

The number of independent reactions was deliberately limited to the peaks/shoulders identified on the averaged DTGA (Figures 5.7). In parallel schemes, species-, element—and constituents-based models have been developed for biomass and carbon/phenolic composites by Torres-Herrador [1, 37] and other researchers, as reviewed by Di Blasi [33]. In this work, these models were avoided to favour simplicity and because of limited information (complementary to TGA) on cork/phenolic material across the literature. Adding complexity without the support of further experimental data on the material characteristics would increase the difficulty of reaching trustworthy results.

Cork 1 (three reactions). Three independent pseudo-reactions were selected to capture the low-temperature onset, the intermediate shoulder around 600 K, and the main peak near 700–750 K (Fig. 5.11). The best-fit parameters (Table 5.1) exhibit a consistent hierarchy of activation energies,  $\mathcal{E}=56.7, 93, 146.6 \text{ kJ mol}^{-1}$ . The global misfit is moderate (S=3.781). At the same time, two structural limitations emerge clearly when comparing heating rates. First, the constant  $F_i$  enforces rate-independent inter-stage partition and residual mass, whereas experiments show a great difference in the mass loss contribution of the first reaction across heating rates and a (small) decrease in char yield with  $\beta$  (Fig. 5.6). Second, the experimental peak shifting with  $\beta$  is larger than what multi-component kinetics can express. Notably,  $\sum_i F_i = 0.84$  implies a 16% residual mass, which underestimates the measured char of Cork 1 and signals a model-form, rather than calibration, limitation.

Table 5.1: Kinetic parameters for Cork 1 (multi-component model). Objective function value: 3.781.

	R1	R2	R3
$F\left[  ext{-} ight]$	0.38	0.06	0.40
n [-]	4.60	1.38	2.68
$\log_{10}(\mathcal{A}_i)~[\text{-}]$	3.96	6.29	9.26
$\mathcal{E}$ [kJ mol <sup>-1</sup> ]	56.68	93.03	146.63

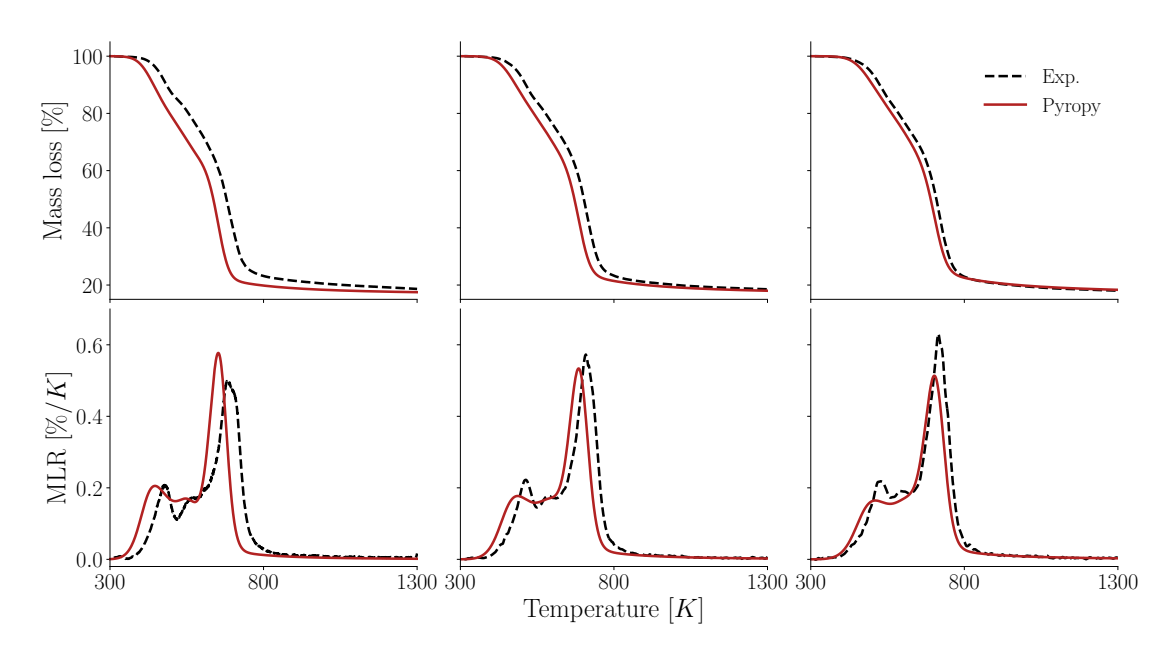


Figure 5.11: Results (red) of parameters optimisation of a 3-reaction, multi-component model for Cork 1.

Cork 2 (two reactions). Cork 2 displays a simpler two-phase DTGA; accordingly, a two-reaction parallel model was implemented (Fig. 5.12). The calibrated parameters (Table 5.2) separate cleanly the broad first stage from the high-temperature peak ( $\mathcal{E} = 136.3 \text{ and } 265.4 \text{ kJ mol}^{-1}$ ).

The objective function (at S=1.94) is lower than the one obtained for Cork 1, and the reconstructed residual  $1-(F_1+F_2)=0.26$  is consistent with the higher char yield experimentally measured for Cork 2 (Fig. 5.6). As for Cork 1, the constancy of  $F_i$  prevents the model from perfectly capturing the observed peak shifts. Nonetheless, these results were deemed satisfactory also due to their reduced complexity and computational cost.

Table 5.2: Kinetic parameters for Cork 2 (multi-component model). Objective function value: 1.94.

	R1	R2
$F\left[  ext{-} ight]$	0.44	0.30
n [-]	6.63	2.81
$\log_{10}(\mathcal{A}_i) \ [\text{-}]$	10.74	17.93
$\mathcal{E} \ [\mathrm{kJ} \ \mathrm{mol}^{-1}]$	136.33	265.39

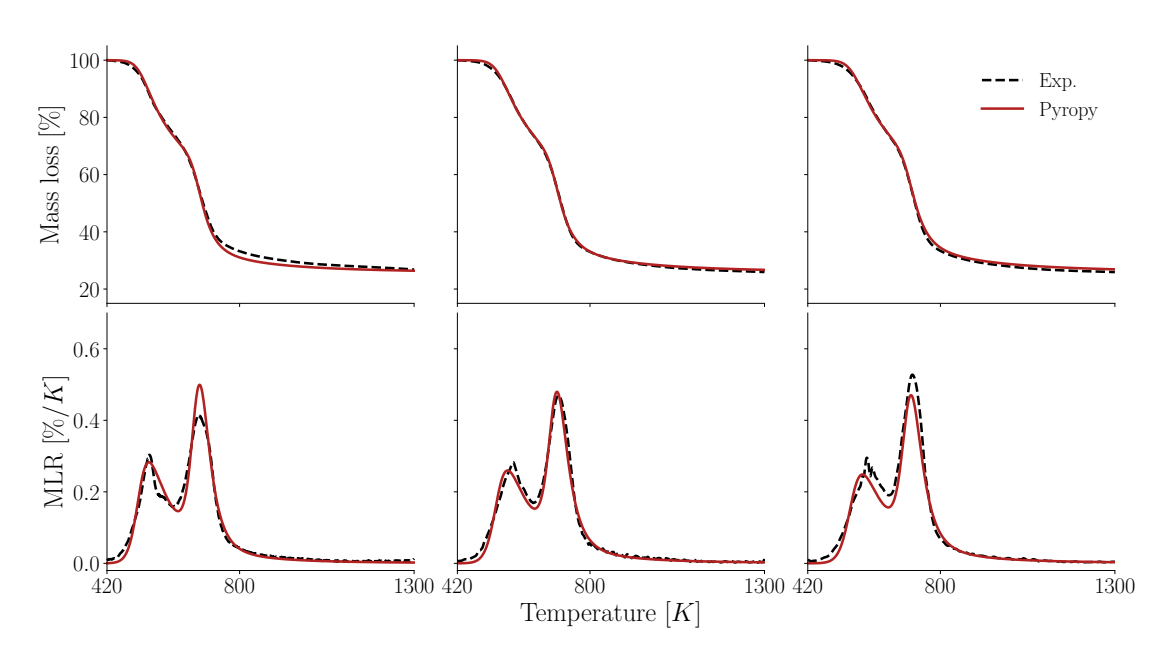


Figure 5.12: Results (red) of parameters optimisation of a 2-reaction, multi-component model for Cork 2.

These results confirm that the parallel (devolatilisation) mechanism is effective for single-rate reconstructions (particularly when DTGA peaks are well separated (Cork 2)) and remains acceptable for more overlapped behaviour (Cork 1). Yet, the assumptions that allow for its reduced complexity (independence and fixed  $F_i$ ) limit its ability to reproduce heating-rate—dependent behaviours (curves shifting and slight yield variations) evidenced by the comparison to the experiments. Increasing the number of pseudoreactions would improve local shape matching but would not remove the structural inability to vary  $F_i$  with  $\beta$ ; therefore, additional complexity is not pursued here. Instead, we proceeded in Section 5.3 to competitive mechanisms for a better, multi-rate ability to fit experimental data of Cork 1.

#### 5.3 Competitive reactions model

Competitive schemes have been shown to capture the heating–rate dependence of carbon/phenolic pyrolysis by allowing a single solid reactant to branch into multiple pathways whose rates,  $k_i(T)$ , compete as temperature rises (Eqs. 3.5–3.7).

For biomass and lignocellulosic solids, analogous branching (often including intermediate solids to delay decomposition onset) is a well-researched practice. An example is reported in Figure 5.13 in which it is reported the competitive model proposed by Bradbury et al. [48]; later generalised by Miller and Bellan [34] and reviewed by Di Blasi [33]. Intermediates provide the necessary time scale separation between low-temperature activation and the subsequent charring or tar-forming pathway.

CELLULOSE 
$$\stackrel{\mathbf{K}_1}{\longrightarrow}$$
 ACTIVE CELLULOSE  $\stackrel{\mathbf{K}_2}{\longrightarrow}$  CHAR+GAS

Figure 5.13: Bradbury's [48] competitive model for pyrolysis of biomass.

Building on the extensive literature on biomass pyrolysis, Torres-Herrador [1, 38] developed a two-branch model (TH) for PICA (Figure 5.14) in which a slow (low-temperature) branch and a fast (high-temperature) branch consume the same solid reactant, reproducing the observed shift of DTGA peaks with  $\beta$ . His work demonstrates that a carry-over from biomass-intended models and carbon/phenolics is possible, allowing for enhanced prospects for a still scarce aerospace-focused literature on competitive mechanisms.

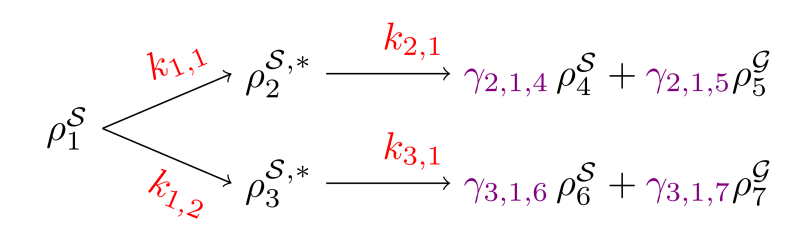


Figure 5.14: Torres-Herrador competitive model (TH) for pyrolysis of PICA®.

Guided by these two lines of work, during this project the competitive scheme of Fig. 5.15 was developed: a biomass-phenolic-inspired surrogate in which a common virgin solid (S1) feeds three branches through activation steps  $(k_1, k_2, k_3)$  that generate intermediate solids (for biomass-like delays) and, downstream, gas/char via  $k_4$ - $k_7$  with yields controlled by  $\gamma_i$ .

# Biomass-phenolic based model to reproduce cork/phenolic pyrolysis

This "biomass/phenolic" competitive model remained intentionally simplified. Biomass literature proves the possibility of associating each constituent of biomass (principally cellulose, hemicellulose, lignin) with an identical competitive branched tree [19, 33, 35]. The branching tree model for each constituent is a derivation of the scheme proposed by Bradbury et al. [48]. Blazquez [19] is the only one, among the scarce literature available, suggesting a similar process for cork, while Sen [18] specifies that cork could be modelled (in parallel) assuming 4 (suberin, polysaccharides, lignin, moisture), 5 (suberin, cellulose, hemicellulose, lignin, moisture) or 6 (suberin I, suberinII, cellulose, hemicellulose, lignin, moisture) subcomponents. It is also important to remember that Bradbury's competitive model for the constituents of biomass pyrolysis (Figure 5.13) might not be suitable to model suberin, which is peculiar if compared to the other constituents of lignocellulose materials [17, 20, 23].

To limit complexity, a single biomass-Bradbury-like branch, rather than four (separate suberin, polysaccharides, lignin, moisture branches), was selected and is presented in Figure 5.15. Yet it still comprised seven reactions and a large set of kinetic and yield parameters to calibrate (Table 5.3).

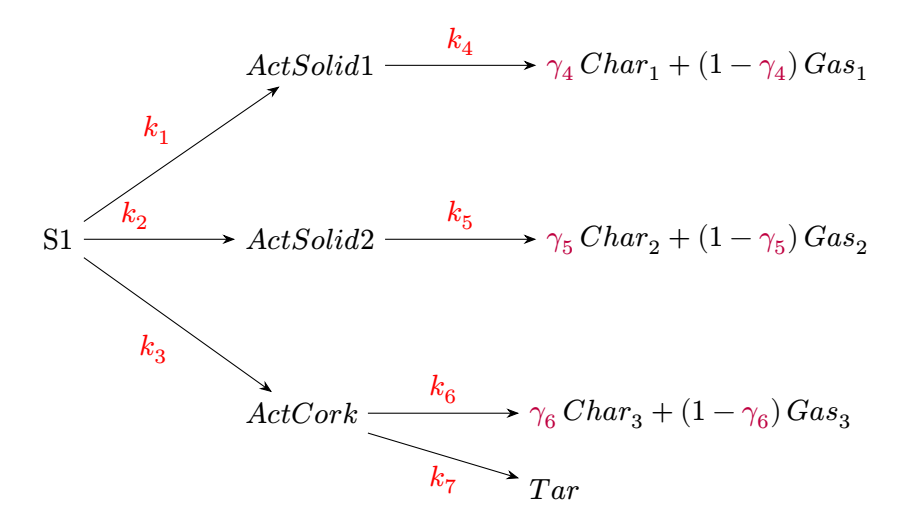


Figure 5.15: Biomass/phenolic competitive reaction scheme derived from Torres-Herrador [38] (phenolic resin) and Miller [34] (biomass).

Despite extensive calibration, the fit quality for Cork 1 (C1) was unsatisfactory (Fig. 5.16). The model captured portions of the DTGA shape but showed limited predictive robustness across heating rates. This is probably due to an over-parameterised mechanism given our restricted calibration set (5, 20 and 40 K/min). In line with Herrador's experience on PICA® [38], reliably constraining such schemes requires sensitivity analysis and possibly a Bayesian treatment to handle parameter non-identifiability and experimental uncertainty—tools we did not explore here. An attempt was made to set

bounds for the deterministic SCE optimisation based on Herrador's Bayesian inference analysis [38], with scarce results. In short, the additional structure (intermediates and extra biomass branch) did not translate into better-fitting behaviour of our cork data.

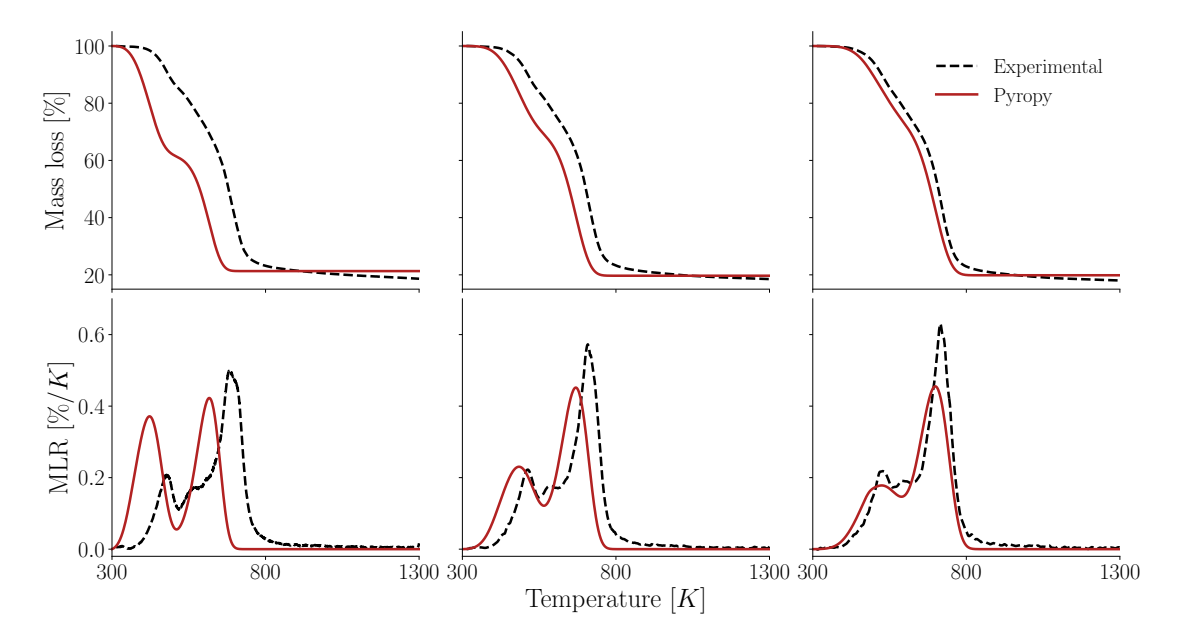


Figure 5.16: Results (red) of optimisation by biomass/phenolic competitive model for Cork 1. TGA above, DTGA under; heating rates (left to right):  $\beta = 5$ , 20, 40 K/min.

Table 5.3: Kinetic parameters for Cork 1 (biomass/phenolic competitive model). Objective function value: 4.27.

	R1	R2	R3	R4	R5	R6	R7
$\log_{10}(\mathcal{A}_i) \ [\text{-}]$	2.43	18.47	0.18	4.09	2.71	1.12	8.22
$\mathcal{E} \; [\mathrm{kJ} \; \mathrm{mol}^{-1}]$	33.81	182.41	18.98	79.88	38.06	31.27	117.40
$\gamma$ [-]	-	-	-	0.89	0.55	0.70	-

#### Regression to the two-branch Herrador model

Given these limitations, we reverted to the original two-branch competitive topology proposed for carbon/phenolics (Figure 5.14) valued for its proven ability to reproduce heating-rate effects of pheolic resins while being biomass-derived. The calibrated result for Cork 1 (Fig. 5.17, Table 5.4) is encouraging for future extensions.

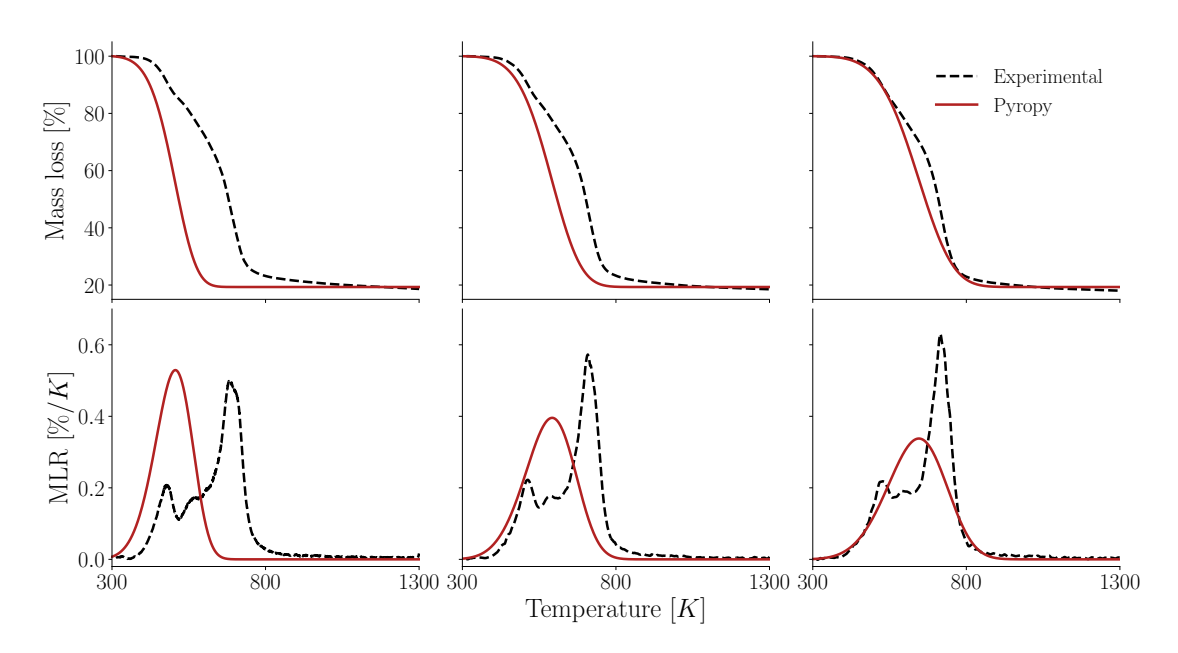


Figure 5.17: Results (red) of optimisation by two-branched competitive model (TH) for Cork 1. TGA above, DTGA under; heating rates (left to right):  $\beta = 5$ , 20, 40 K/min.

Only one branch effectively activates over the tested heating rates ( $\beta = 20$ –40 K/min), yet the model still reproduces the observed phenomenology: DTGA peak shift with  $\beta$  and the correct temperature start/stop of mass loss. This is a direct consequence of the competitive structure (matrix form, Eq. 3.7), where pathway selection emerges from the Arrhenius competition and does not require fixed F coefficients. The "fast" branch parameters were identified with large activation energy and pre-exponential factor (R2 and R4 in Table 5.4, but they remained largely inactive within our calibration window.

Table 5.4: Kinetic parameters for Cork 1 (two-branch competitive model(TH)). Objective function value: 6.16.

	R1	R2	R3	R4
$\log_{10}(\mathcal{A}_i) \ [\text{-}]$	5.31	20.57	0.30	12.76
$\mathcal{E} \; [\mathrm{kJ} \; \mathrm{mol}^{-1}]$	10.16	181.94	31.16	22.18
$\gamma$ [-]	-	-	0.81	0.47

Although the biomass/phenolic scheme achieved a lower objective value on Cork 1 than the two-branch fit (TH model), its high computational cost and poor extrapolative behaviour argue for the simpler Herrador topology as a baseline. This choice is also consistent with best practice in kinetic modelling: start from the smallest mechanism that captures the salient physics, then add detail if supported by data.

#### Heating-rate coverage and the 5 K/min issue

The simplified competitive model behaves as expected at  $\beta=20$  and 40 K/min: the single active branch reproduces the progressive peak shift and associated changes in apparent char yield (Sec. 3.2). However, a persistent mismatch appears at  $\beta=5$  K/min for Cork 1: neither the seven-reaction scheme nor a simple parallel fit fitted the 5 K/min data satisfactorily, reproducing the DTGA/TGA. The fact that the same issue does not arise for Cork 2, for which  $\beta=5$  K/min is well captured, suggests that the competitive framework is sound and that the discrepancy is material or data-specific rather than structural. Even if experimental data (as discussed in Section 5.1) recorded in this campaign were consistent with the literature. At present, the root cause remains unidentified.

#### Concluding remarks

Overall, the study indicates that (i) introducing biomass-style intermediates is conceptually feasible for cork (even if not originally intended due to the presence of suberin) but becomes under-constrained with the limited  $\beta$  range experimented; (ii) the two-branch Herrador model provides a compact, physically consistent baseline that already reproduces the  $\beta$ -dependent phenomenology at 20–40 K/min. Improving the activation of the fast branch (either by targeted parameter refinement or by augmenting the calibration set with higher- $\beta$  data) should further increase fidelity and enable individual solids yield shifts with  $\beta$  as observed in competitive systems for both phenolics and biomass. Individual solids/components' behaviour was tracked during the presented optimisations, but results needed refinement and were not yet significant to this work. Where data quantity/quality permit, a Bayesian calibration similar to that performed for PICA<sup>®</sup> [38] would be the best route to improve parameter contribution understanding and quantify uncertainty on predictions.

Cork 1 results. The biomass/phenolic competitive model (Fig. 5.16) demonstrates the intended pathway structure but yields a fragmented fit across the experimentally tested  $\beta$ . The TH two-branch model (Fig. 5.17), despite activating a single branch, captures the DTGA peak positions and the onset/ending of mass loss with promising accuracy. The persistent misfit at 5 K/min is confined to Cork 1; Cork 2 does not exhibit this behaviour, reinforcing the suitability of the simplified competitive baseline for the dataset at hand.

## Chapter 6

# Conclusions and future developments

Objective 1. Establish a reliable calibration basis at laboratory heating rates. A multirate TGA/DTGA dataset was built for two cork/phenolic ablators (Cork 1 and Cork 2) at 5, 20 and 40 K/min. The campaign showed excellent repeatability across repetitions and rates and consistency with experimental data from the literature. A dedicated run in a sealed glovebox confirmed that the initial low-temperature mass loss observed for Cork 2 was moisture volatilisation and validated that operating in ambient conditions did not bias the main pyrolysis trends. Controlled storage nevertheless improved the accuracy of initial mass assessment. After normalisation and smoothing, the averaged curves provided a consistent basis for parameter identification.

Objective 2. Determine a kinetic mechanism that supports the temperature- and time-dependent behaviour of cork/phenolic materials.

Parallel (multi-component) schemes. For Cork 1, a three-reaction model reproduced the low-temperature onset, the intermediate shoulder and the main peak, while for Cork 2, a two-reaction model captured its two-phase DTGA structure. Within 20–40 K/min, these schemes matched TGA/DTGA with low misfit and returned physically plausible activation energies and mass-loss fractions. As expected, structural limitations emerged: fixed mass-loss fractions ( $F_i$ ) enforce rate-independent partitions and residuals, and the magnitude of peak shifting with ( $\beta$ ) is under-predicted. A persistent mismatch at 5 K/min for Cork 1 could not be removed by restricting calibration to that rate alone, indicating limited cross-rate generality of a purely parallel formulation for that material.

Competitive schemes. A biomass/phenolic-inspired competitive network with intermediates was prototyped to allow pathway selection with  $(\beta)$ . Despite reproducing portions of the DTGA shape, it proved under-constrained by the available  $(\beta)$ -span and over-parameterised for deterministic optimisation. Regressing to a

simpler two-branch competitive topology (in the spirit of Herrador's model for carbon/phenolics) yielded a compact, stable baseline: one branch sufficed to reproduce (i) onset and cessation of mass loss and (ii) the observed peak shift between 20 and 40 K/min for Cork 1. The "fast" branch remained mostly inactive within the explored laboratory rates, signalling where additional high- $(\beta)$  data are needed.

Tooling. Pyropy was adapted to the present task (robust TXT parsing/averaging, explicit Jacobian hand-off to the stiff IVP solver, safeguarded SCE settings), enabling reproducible calibrations for both formulations.

This objective is partially achieved: a minimal competitive baseline that captures ( $\beta$ )-dependent phenomenology at 20–40 K/min is established, and parallel models provide accurate reconstructions within-rate. However, truly robust competitive parameters require additional information.

**Objective 3.** Compare Cork 1 and 2 under common experimental conditions. Under identical protocols, the two ablators showed clear differences:

Residual mass (char yield). Cork 2 consistently produced ( $\square 26\%$ ) residual mass versus ( $\square 18\%$  - 19%) for Cork 1 (all rates), pointing to a higher effective resin fraction and/or different cork phase behaviour.

Reactions onset and stages. Cork 1 displayed a three-stage evolution with an intermediate reaction around  $\approx 600$  K. Cork 2 exhibited two main stages, with a broader first stage starting later and a major peak near 680–720 K. Cork 2 also showed moisture volatilisation-driven mass loss ( $\approx 400$  K) when sample were stored under ambient conditions.

Heating-rate effects. Both materials showed the expected shift of DTGA peaks to higher temperatures with increasing ( $\beta < 100 \text{ K/min}$ ), and small, rate-dependent variations of residual mass. The 5 K/min mismatch during multi-component optimisation, noted for Cork 1, did not occur for Cork 2.

#### 6.1 Recommendations for future developments

The results presented define a clear path to strengthen model fidelity and extend validity towards flight-representative conditions for cork/phenolic ablators. Three lines of work are especially promising: improving parameter identifiability and quantifying uncertainty; acquiring more informative experimental data and material descriptors; and refining both the reaction mechanism and the calibration workflow.

A first priority is to assess how strongly each kinetic and yield parameter influences the observables used for calibration. A global sensitivity analysis would rank parameters by influence on mass loss, DTGA peak temperatures and widths, residual mass, and the amount of shifting. Building on that, Bayesian calibration should replace point estimation. SCE fits can be combined with posterior inference or variational methods to produce plausible intervals for  $\mathcal{E}$ ,  $\mathbb{A}$ , and yield fractions, and to propagate uncertainty. In closely related carbon/phenolic systems, this approach proved decisive in stabilising competitive kinetics and provided useful information for the present work [1].

A significant amount of experimental data would be required. Confirming the cork to resin mass ratio would reduce ambiguity when partitioning yields among branches. On the gas side, coupling TGA with Elemental Analysis (EA) and/or Fourier transform infrared spectroscopy (FTIR) to obtain species- or element-resolved volatile yields as functions of temperature and heating rate would enable element/species-balanced multi-component or competitive models; as previously done for phenolic materials [26]. Extending the heating-rate span to  $\beta \geq 100~K/min$  should activate the fast competitive branch and constrain its Arrhenius parameters over the range relevant to entry heating. DSC measurements would characterise heat capacity, while isothermal TGA would isolate activation steps. Finally, microstructure observations (such as the one presented by Foster [22] for SLAs) would document pore evolution and final residual composition. These features impact pathway selection and char-yield formation in cork/phenolics.

Kinetically, the current two-branch competitive baseline should be retained as a backbone. A biomass-like branch could be added once good results are achieved with simpler reaction schemes. Until additional TGA data are recorded, more complex trees would be under-constrained.

The present work can address the initial research question as follows: a rate-aware mechanism calibrated on multi-rate TGA/DTGA already reproduces the laboratory phenomenology of cork/phenolic pyrolysis at 20–40 K/min with a compact competitive topology, and parallel schemes provide accurate within-rate reconstructions. For a broader, flight-relevant heating-rate spectrum, the model must be tested by sensitivity and Bayesian analyses with the support of more informative data. For example, confirmed composition, gas-phase species or element yields, and higher- $\beta$  TGA coupled with complementary diagnostics. These steps are concrete and feasible, and they will convert the present baseline into a predictive, uncertainty-quantified tool suitable for TPS design and analysis.

# **Bibliography**

- [1] F. Torres-Herrador. "Thermal response of carbon composites submitted submitted to high temperatures: Application to atmospheric entry." PhD thesis. Vrije Universiteit Brussel, The von Karman Institute for Fluid Dynamics, Ghent University, 2022.
- [2] F. J. Torres-Herrador. "Thermal Characterization of Ablative Materials." Master's thesis. Universidad Politécnica de Valencia, 2018.
- [3] B. Helber et al. Cork P50 and TPS3L Ablation Experiments for the Demise Observation Capsule Including an Adhesive Bonded TPS3L Structure. Aeronautics and Aerospace Department, von Karman Institute for Fluid Dynamics.
- [4] I. Sakraker, B. Helber, and O. Chazot. "Experimental Characterization of Cork Based Thermal Protection Material P50." English. In: 8th European Symposium on Aerothermodynamics for Space Vehicles. 8th European Symposium on Aerothermodynamics for Space Vehicles. 8th European Symposium on Aerothermodynamics for Space Vehicles; Conference date: 02-03-2015 Through 06-03-2015. Lisbon: European Space Agency, 2015.
- [5] I. Sakraker, O. Chazot, and J. P. Carvalho. "Performance of cork-based thermal protection material P50 exposed to air plasma." In: *CEAS Space Journal* 14.2 (Apr. 1, 2022), pp. 377–393. DOI: 10.1007/s12567-021-00395-z.
- [6] C. Miccoli. "Detailed Modeling of Cork-Phenolic Ablators in Preparation to the Post-Flight Analysis of the QARMAN Re-Entry CubeSat." Master's thesis. Politecnico di Torino, July 28, 2020. 151 pp.
- [7] QARMAN QubeSat for Aerothermodynamic Research and Measurements on AblatioN. The von Karman Institute for Fluid Dynamics. URL: https://www.vki.ac.be/index.php/qarman-home (visited on 10/12/2025).
- [8] F. Portugal. ESA's IXV Project. Amorim Cork Solutions. URL: https://amorim.corksolutions.com/en-us/knowledge-center/case-studies/ixv-project/(visited on 09/09/2025).
- [9] Amorim Cork Solutions. Brochure "Reinventing thermal protection in aerospace applications". Amorim Cork Solutions. URL: https://amorimcorksolutions.com/en-us/ (visited on 10/03/2025).

- [10] Draco mission made for destruction. European Space Agency. URL: https://wwww.esa.int/Space\_Safety/Draco\_mission\_made\_for\_destruction (visited on 10/12/2025).
- [11] A. Perin. Characterization of Specific Heat and Decomposition Rates of Composite Overwrapped Pressure Vessel material used for Space Missions. Tech. rep. The von Karman Institute for Fluid Dynamics, 2024.
- [12] C. Miccoli et al. "Detailed Modeling of Cork-Phenolic Ablators in Preparation for the Post-flight Analysis of the QARMAN Re-entry CubeSat." In: *Aerotecnica Missili & Spazio* 100.3 (Sept. 1, 2021), pp. 207–224. DOI: 10.1007/s42496-021-00084-4.
- [13] V. A. Monteiro and M. T. Mendes. Numerical Simulations of the QARMAN Thermal Protection System in High Enthalpy Flows. 2021.
- [14] D. D'Ambrosio. *Hypersonic Aerothermodynamics lectures*. Aerospace Engineering Master Course notes, Politecnico di Torino, Italy. Lecture notes. 2019.
- [15] A. Amar, N. Calvert, and B. Kirk. "Development and Verification of the Charring Ablating Thermal Protection Implicit System Solver." In: 49th AIAA Aerospace Sciences Meeting including the New Horizons Forum and Aerospace Exposition. Aerospace Sciences Meetings. American Institute of Aeronautics and Astronautics, Jan. 4, 2011. DOI: 10.2514/6.2011-144.
- [16] M. Natali et al. "Thermal degradation of phenolics and their carbon fiber derived composites: A feasible protocol to assess the heat capacity as a function of temperature through the use of common DSC and TGA analysis." In: *Polymer Degradation and Stability* 195 (Jan. 1, 2022), p. 109793. DOI: 10.1016/j.polymdegradstab.2021.109793.
- [17] F. Ghonjizade-Samani et al. "The Components' Roles in Thermal Stability and Flammability of Cork Powder." In: *Materials* 16.10 (Jan. 2023). Publisher: Multi-disciplinary Digital Publishing Institute, p. 3829. DOI: 10.3390/ma16103829.
- [18] A. U. Şen et al. "Pyrolysis kinetics and estimation of chemical composition of Quercus cerris cork." In: *Biomass Conversion and Biorefinery* 12.11 (Nov. 1, 2022). Company: Springer Distributor: Springer Institution: Springer Label: Springer Publisher: Springer Berlin Heidelberg, pp. 4835–4845. DOI: 10.1007/s13399-020-00964-y.
- [19] G. Blázquez et al. "Study of the kinetic parameters of thermal and oxidative degradation of various residual materials." In: *Biomass and Bioenergy* 124 (May 1, 2019), pp. 13–24. DOI: 10.1016/j.biombioe.2019.03.008.
- [20] A. Şen et al. "Thermal behaviour of cork and cork components." In: *Thermochimica Acta* 582 (Apr. 20, 2014), pp. 94–100. DOI: 10.1016/j.tca.2014.03.007.
- [21] A. M. Ribeiro et al. "Thermogravimetric analysis of high-density cork granules using isoconversional methods." In: *Energy Reports*. The 8th International Conference on Energy and Environment Research "Developing the World in 2021 with Clean and Safe Energy" 8 (June 1, 2022), pp. 442–447. DOI: 10.1016/j.egyr.2022.01.100.

- [22] C. W. Foster, S. Oruganti, and F. Panerai. "Super-resolved microstructure of pyrolyzing superlight ablators." In: npj Materials Degradation 9.1 (Feb. 5, 2025). Publisher: Nature Publishing Group, p. 9. DOI: 10.1038/s41529-025-00556-z.
- [23] N. Cordeiro et al. "Cork suberin as a new source of chemicals: 2. Crystallinity, thermal and rheological properties." In: *Bioresource Technology* 63.2 (Feb. 1, 1998), pp. 153–158. DOI: 10.1016/S0960-8524(97)00073-4.
- [24] E. H. Stokes. "Kinetics of pyrolysis mass loss from cured phenolic resin." In: *Journal of Thermophysics and Heat Transfer* (1995). DOI: 10.2514/3.667.
- [25] B. K. Bessire, S. A. Lahankar, and T. K. Minton. "Pyrolysis of Phenolic Impregnated Carbon Ablator (PICA)." In: ACS Applied Materials & Interfaces 7.3 (Jan. 28, 2015). Publisher: American Chemical Society, pp. 1383–1395. DOI: 10.1 021/am507816f.
- [26] B. K. Bessire and T. K. Minton. "Decomposition of Phenolic Impregnated Carbon Ablator (PICA) as a Function of Temperature and Heating Rate." In: ACS Applied Materials & Interfaces 9.25 (June 28, 2017). Publisher: American Chemical Society, pp. 21422–21437. DOI: 10.1021/acsami.7b03919.
- [27] Thermal Protection Materials Branch Low Density Ablators NASA. Section: General. Apr. 10, 2023. URL: https://www.nasa.gov/general/thermal-protection-materials-branch-low-density-ablators/ (visited on 10/12/2025).
- [28] F. Torres-Herrador et al. "Comparison between traditional and competitive reaction models for the pyrolysis of high temperature aerospace materials." In: AIAA Aviation 2019 Forum. AIAA AVIATION Forum. American Institute of Aeronautics and Astronautics, June 14, 2019. DOI: 10.2514/6.2019-3361.
- [29] L. Nowicki and M. Markowski. "Kinetic analysis of thermogravimetric data collected from bigger samples." In: Chemical and Process Engineering 33.1 (Jan. 1, 2012). DOI: 10.2478/v10176-012-0008-z.
- [30] F. J. Torres-Herrador. Experimental Characterization and Simulation of Pyrolysis Phenomenon: From Carbon Composite Ablators to Pacific Islands Plant Biomass. Research master. von Kármán Institute for Fluid Dynamics, 2017.
- [31] Z. Wang et al. "Thermal Decomposition and Moisture Absorption Kinetic Analysis of Spaceflight Cork Board." In: *Academic Journal of Engineering and Technology Science* 4.6 (Oct. 20, 2021). Publisher: Francis Academic Press. DOI: 10.25236/A JETS.2021.040603.
- [32] E. Smith et al. "Thermal/ablation model of low density cork phenolic for the Titan IVStage I engine thermal protection system." In: 27th Thermophysics Conference. Fluid Dynamics and Co-located Conferences. American Institute of Aeronautics and Astronautics, July 6, 1992. DOI: 10.2514/6.1992-2905.
- [33] C. Di Blasi. "Modeling chemical and physical processes of wood and biomass pyrolysis." In: *Progress in Energy and Combustion Science* 34.1 (Feb. 1, 2008), pp. 47–90. DOI: 10.1016/j.pecs.2006.12.001.

- [34] R. Miller and J. Bellan. "A Generalized Biomass Pyrolysis Model Based on Superimposed Cellulose, Hemicelluloseand Liqnin Kinetics." In: *Combustion Science and Technology* 126.1 (July 1, 1997). Publisher: Taylor & Francis, pp. 97–137. DOI: 10.1080/00102209708935670.
- [35] K. McLarney-Popham. "Computational Modeling of the Heat Treatment of White Oak Bound for Spirit Maturation." In: *Theses and Dissertations-Chemical and Materials Engineering* (Jan. 1, 2025). DOI: https://doi.org/10.13023/etd.2025.148.
- [36] F. Torres-Herrador et al. "A high heating rate pyrolysis model for the Phenolic Impregnated Carbon Ablator (PICA) based on mass spectroscopy experiments." In: Journal of Analytical and Applied Pyrolysis 141 (Aug. 1, 2019), p. 104625. DOI: 10.1016/j.jaap.2019.05.014.
- [37] F. Torres-Herrador et al. "Multicomponent Pyrolysis Model for Thermogravimetric Analysis of Phenolic Ablators and Lignocellulosic Biomass." In: *AIAA Journal* 58.9 (Sept. 2020). Publisher: American Institute of Aeronautics and Astronautics, pp. 4081–4089. DOI: 10.2514/1.J059423.
- [38] F. Torres-Herrador et al. "Competitive kinetic model for the pyrolysis of the Phenolic Impregnated Carbon Ablator." In: Aerospace Science and Technology 100 (May 1, 2020), p. 105784. DOI: 10.1016/j.ast.2020.105784.
- [39] Amorim Cork Solutions. Amorim TPS: Ablative Thermal Protection Solutions for the Aerospace Industry. Amorim Cork Solutions. URL: https://amorimcorksolutions.com/en-us/materials-applications/aerospace/ (visited on 10/02/2025).
- [40] R. A. Graves and T. E. Walton Jr. Free-flight test results on the performance of cork as a thermal protection material. District of Columbia, United States: Washington, D.C.: National Aeronautics, Space Administration: [For sale by the Clearinghouse for Federal Scientific, and Technical Information, Springfield, Virginia], 1964.
- [41] F. Torres-Herrador et al. "Determination of heat capacity of carbon composites with application to carbon/phenolic ablators up to high temperatures." In: *Aerospace Science and Technology* 108 (Jan. 1, 2021), p. 106375. DOI: 10.1016/j.ast.2020.106375.
- [42] F. Torres-Herrador. Pyropy. original-date: 2022-06-28T14:53:28Z. Sept. 17, 2025.
- [43] C. Lautenberger and A. C. Fernandez-Pello. "Optimization Algorithms for Material Pyrolysis Property Estimation." In: *Fire Safety Science* 10 (2011), pp. 751–764.
- [44] Thermal Protection Systems. Amorim Cork Composites Asia. URL: https://www.amorimasia.com/uploads/4/8/0/0/48004771/tps\_pp\_04\_07\_2008ac.pdf (visited on 09/10/2025).
- [45] F. Torres-Herrador et al. "Study of the degradation of epoxy resins used in space-craft components by thermogravimetry and fast pyrolysis." In: *Journal of Analytical and Applied Pyrolysis* 161 (Jan. 1, 2022), p. 105397. DOI: 10.1016/j.jaap.2021.105397.

- [46] G. F. Sykes. Decomposition characteristics of a char-forming phenolic polymer used for ablative composites. Tech. rep. NASA, 1967.
- [47] F. Jafari, R. Eslami-Farsani, and S. M. R. Khalili. "Optimization of Mechanical and Thermal Properties of Elastomer Modified Carbon Fibers/Phenolic Resin Composites." In: Fibers and Polymers 22.7 (July 1, 2021). DOI: 10.1007/s12221-021-0934-9.
- [48] A. G. W. Bradbury, Y. Sakai, and F. Shafizadeh. "A kinetic model for pyrolysis of cellulose." In: *Journal of Applied Polymer Science* 23.11 (1979), pp. 3271–3280. DOI: 10.1002/app.1979.070231112.